New insights into Holocene hydrology and temperature from lipid biomarkers in western Mediterranean alpine wetlands

Jaime L. Toney [a,†], Antonio García-Alix [a,b,c,†,*], Gonzalo Jiménez-Moreno [b], R. Scott Anderson [d], Heiko Moossen [a,e], Osamu Seki [f]

[a] School of Geographical and Earth Sciences, University of Glasgow, UK.
[b] Department of Stratigraphy and Paleontology, University of Granada, Granada, Spain. Current address of Antonio García-Alix.
[c] Instituto Andaluz de Ciencias de la Tierra (IACT), CISC-UGR, Armilla, Spain.
[d] School of Earth and Sustainability, Northern Arizona University, Flagstaff, AZ, USA.
[e] MaxPlanck-Institute for Biogeochemistry, Hans Knoell street 10, 07745 Jena, Germany. Current address of Heiko Moossen.
[f] Institute for Low Temperature Science, Hokkaido University, Japan.

[†] Indicates equal author contributions

* Corresponding author: Antonio Garcia-Alix: agalix@ugr.es

ABSTRACT

Alpine regions of the Mediterranean realm are among the most climatically sensitive areas in the world. Thus, alpine wetlands from the southern Iberian Peninsula, in the westernmost part of the Mediterranean region, are highly sensitive sensors of environmental changes. Difficulties have surfaced in separating controls by temperature and/or precipitation in previous paleoenvironmental studies from alpine environments in this area. We present a Holocene biomarker record (*n*-alkanes and long-chain diols) from a high elevation lake, Laguna de Río Seco (LdRS), in the south of the Iberian Peninsula, which contributes to the identification of these forcing mechanisms. The hydrological history of the area, primarily water availability and evapotranspiration, is reconstructed by means of the *n*-alkane record, including the indices of average chain length, portion aquatic, and carbon preference index, as well as hydrogen isotopes (δD) of aquatic (δD_{aq}) and terrestrial (δD_{wax}) *n*-alkanes. Temperatures are also estimated using the algae derived long-chain diols. We interpret δD_{aq} and δD_{wax} fluctuations as showing changes in the source and amount of precipitation throughout the LdRS record. An Atlantic precipitation source appears to have predominated during the early-middle Holocene, but an occasional Mediterranean influence with an isotopic enrichment in precipitation is detected in the middle-late Holocene that is likely related to the setting of the current atmospheric pattern in southeastern Iberia under the joint control of the North Atlantic Oscillation (NAO) and the Western Mediterranean dynamics, such as the Western Mediterranean Oscillation (WeMO). Our new record from LdRS is consistent with a generalized trend of a humid early-middle Holocene with low temperature variability, evolving towards an arid middle-late Holocene with abrupt temperature changes. In addition to these long-term trends during the last ~10,500 years, two phases of climate instability, evidenced by abrupt depletions in δD_{aq}, have been identified at the end of these periods, one between ~6500 and 5500 cal. yr BP and another in the last ~500 years. These episodes would represent strengthened winter cold conditions that favoured the persistence of snowpack and frozen soil in the catchment, causing reduced terrestrial plant growth and low lake evaporation. According to the long-chain diol record, temperatures during these phases were relatively low, but experienced abrupt increases at the end of each period.

KEYWORDS: Holocene; *n*-alkanes; long-chain diols; Sierra Nevada; Southern Iberian Peninsula

1. Introduction

In our changing world where rapidly shifting climatic conditions affect ecosystems in multiple ways, it is especially important to assess and document environmental responses in regions that are sensitive to climate change. This is critical for projecting future scenarios and developing appropriate management strategies, for example, to prevent the loss or migration of endemic species, which in many cases are endangered, often very specialised, and among the first to suffer the effects of environmental change. A case in point is the Sierra Nevada region in the western Mediterranean, one of the most important mountain ranges in southwestern Europe (Menéndez et al., 2014), and a region particularly sensitive to climate change (Giorgi, 2006; IPCC, 2014; Lionello et al., 2006). This range, with peaks exceeding 3000 meters above sea level (masl), has historically been a natural refuge for several endemic (Blanca, 2001; Van Swaay and Warren, 1999) and vulnerable taxa, as was the case of the southernmost European woolly mammoth, which sheltered in the lowest wetlands during cold and dry Heinrich Stadials (Álvarez-Lao et al., 2009; García-Alix et al., 2012a).

About 50 small, mostly oligo-mesotrophic high-alpine lakes and peatlands of glacial origin have been documented in the Sierra Nevada (Pulido-Villena et al., 2005). These fragile sites, occurring primarily above 2500m elevation, are *in-vivo* laboratories for ecological studies and their biogeochemical responses are very sensitive to climatic and environmental variations (Jiménez et al., 2018; Mladenov et al., 2011; Pulido-Villena et al., 2005; Reche et al., 2009). This also makes them sensitive to past environmental and climatic changes, as it has been shown from pollen, charcoal, major and trace elements, and organic proxies, among others (Anderson et al., 2011; Garcia-Alix et al., 2017; García-Alix et al., 2018; García-Alix et al., 2012b; García-Alix et al., 2020; Jiménez et al., 2019; Jiménez et al., 2018; Jiménez-Espejo et al., 2014; Jiménez-Moreno and Anderson, 2012; Jiménez-Moreno et al., 2013; Mesa-Fernández et al., 2018; Ramos-Román et al., 2016). These studies determined that warm and wet climates occurred during the early-middle Holocene, with the highest Holocene lake levels in the Sierra Nevada and a minimal influence of aeolian Saharan dust inputs, followed by an aridity trend during the middle-to-late Holocene. However, many specific and significant questions remain unresolved, including (1) how were these alpine wetlands affected by changes in precipitation, evaporation and temperature during the middle Holocene transition period?; (2) how did the hydrologic changes influence the aquatic and terrestrial environments?; and (3) were the observed changes related to seasonality or perhaps changes in precipitation source through time? Thus, despite the wealth of paleoclimate reconstructions from these high alpine lakes, there is still a lack of data that characterizes the paleohydrology, evaporation-to-precipitation balance, and the temperature

variability. Characterizing these additional components will allow for a better understanding of what controls the development of lacustrine or peatland conditions, as well as the vegetation of the area. In this paper, we use the latest biomarker techniques to characterise long-chain *n*-alkanes and algae-derived, long-chain diols from the sedimentary record of Laguna de Río Seco (LdRS) to maximize the ecological and climatic interpretations already gained from previous studies.

1.1 Regional setting

The Sierra Nevada range is located in the southeastern Iberian Peninsula, less than 30km north of the Mediterranean Sea. It is characterized by a typical Mediterranean climate with scarce annual precipitation. Summers are hot and dry, with occasional precipitation during September marking the transition to autumn. Summers are primarily influenced by subtropical climate dynamics related to the strengthening of the Azores high-pressure system. Most of the annual precipitation occurs during the cold-temperate season, is sourced from the Atlantic Ocean (Araguas-Araguas and Diaz Teijeiro, 2005), and is mainly influenced by North Atlantic climatic processes, such as the polar cyclone (Iceland Low), and hence the North Atlantic Oscillation (NAO) (Lionello et al., 2006; Millán et al., 2005). The NAO primarily influences winter precipitation in the western Mediterranean, and has little effect on winter temperatures (Lionello et al., 2006; Trigo et al., 2006). However, the contribution of Mediterranean precipitation from late spring to early autumn, potentially influenced by the Western Mediterranean Oscillation (WeMO) (Moreno et al., 2014), is also important near the Iberian Mediterranean coast and in the eastern side of the Iberian Peninsula (Araguas-Araguas and Diaz Teijeiro, 2005; Millán et al., 2005; Moreno et al., 2014). Hence, inter- and intra-annual variations in the NAO (Hurrell, 1995) and WeMO mode (Martin-Vide and Lopez-Bustins, 2006; Moreno et al., 2014) affect climates in the western Mediterranean. Previous paleoclimatic studies show that persistent periods (decades or centuries) of prevailing NAO modes could have also characterised the climate in the north Atlantic region during the Holocene (Fletcher et al., 2013; Moossen et al., 2015; Olsen et al., 2012; Trouet et al., 2009); nevertheless, long-term Holocene trends of the Western Mediterranean dynamics and their effect on climate still need to be further investigated (Moreno et al., 2014).

Contrasting climate conditions between low and high elevation sites in the study area also need to be considered. At lower elevations, e.g. Padul town (37°1'N, 3°37'W; 760 masl), the mean annual air temperature (MAAT) is ~14.4ºC with a range from ~26°C in the summer to ~7°C in the winter, and with the majority of the annual rainfall (445mm) falling between October and

March (Spanish National Weather Agency - AEMet Open Data, 2020). Meteorological records are scarce above 2000 masl in the Sierra Nevada (García-Alix et al., 2018) and the longest climatic series comes from a discontinuous record from 1965 to 1993 (Prado Llano – Albergue University at 2500 masl) registering a MAAT of ~4.4ºC, ranging from ~18ºC in summer to ~-4ºC in winter. The annual precipitation at this elevation ranges from ~700 to 750 mm and mainly falls as snow between October and May (Observatorio del cambio global de Sierra Nevada, 2020; Spanish National Weather Agency - AEMet Open Data, 2020).

The period of snow cover in the Sierra Nevada alpine areas has registered a 4-day shortening from 2000 to 2014 coeval with a gradual retraction of relict ice and permafrost (Zamora et al., 2016). Nevertheless, a recent study suggested that cold and snow events have not decreased in the Mediterranean region during the last 60 years in spite of temperature rising, as a consequence of enhanced convective precipitation (D'Errico et al., 2019). There is an intense debate about the potential triggers of these cold and snow events in European mid-latitudes during the Industrial Period such as the combined effect of sea-ice reduction and the feedback mechanism of the northern Hemisphere atmospheric dynamics (e.g. the NAO and the Arctic Oscillation) (Ambaum et al., 2001; Liu et al., 2012). For example, some studies showed that the effect of the sea ice reduction along with the coupling and decoupling between these northern Hemisphere atmospheric dynamics could give rise to cold and rainy winters in the Mediterranean Basin (Grassi et al., 2013), enhancing snow precipitation in southern Iberian mountains (Báez et al., 2013). However, other studies do not show any significant impact of sea ice variations on mid latitude climates (Koenigk et al., 2019; Vihma, 2014), and point to the NAO as the most relevant mode for Northern Hemisphere climate variability (Ambaum et al., 2001). In this regard, the snow cover in the Iberian mountains, including the Sierra Nevada, is greater and longer lasting during negative winter NAO phases (Alonso-González et al., 2020), confirming the important influence of the NAO on the climate of the Sierra Nevada mountains (Garcia-Alix et al., 2017; López-Moreno et al., 2011; Ramos-Román et al., 2016).

Cold and semi-arid conditions predominate at elevations above 2500 masl and cause minimal soil development on the mica-schist bedrock. These alpine environments are characterised by the presence of crioromediterranean flora with tundra-like open grassland and plants with basal rosettes (Valle, 2003), such as *Festuca clementei* Boiss*, Hormathophylla purpurea* (Lagasca and Rodriguez) Küpfer*, Erigeron frigidus* Boiss*, Saxifraga nevadensis* Boiss*, Viola crassiuscula* Bory*,* and *Linaria glacialis* Boiss (see Anderson et al., 2011 for vegetation description of the elevational trend). The present-day treeline in the

Sierra Nevada is located at ~2550 masl as a consequence of human-induced reforestation, but the natural treeline could be lower since natural populations of trees occur at ~2100 masl (Anderson et al., 2011). Pollen records suggest that past changes in temperature and precipitation caused major vegetation shifts throughout the Holocene (Anderson et al., 2011; Jiménez-Moreno and Anderson, 2012; Jiménez-Moreno et al., 2013; Mesa-Fernández et al., 2018; Ramos-Román et al., 2016)

In this study we analyse the biomarker record from an alpine lake in the Sierra Nevada, Laguna de Río Seco (LdRS), (37°02.43′N, 3°20.57′W, ~3020 masl), which is located in a south-facing glacial cirque basin (Fig. 1). It has a maximum depth of ~3 m, a surface area of 0.42 ha, and a small catchment basin (9.9 ha) (Morales-Baquero et al., 1999). Previous studies from the LdRS sediment record include a detailed age model, pollen, charcoal, major and trace elements, and carbon and nitrogen isotopic analyses (Anderson et al., 2011; García-Alix et al., 2018; Garcia-Alix et al., 2013; Jiménez et al., 2019; Jiménez et al., 2018; Jiménez-Espejo et al., 2014), as well as a high resolution long-chain diol study throughout the Common Era (García-Alix et al., 2020). Therefore, the results from the organic geochemical biomarkers discussed in this paper compare, contrast, and add value to those from the previously studied proxies in the same record, providing new insights into drivers of change in these high-altitude ecosystems.

1.2 n-Alkane distributions as proxies for vegetation characteristics

n-Alkanes have become a widely used organic geochemical tool for understanding past climate change (Diefendorf et al., 2011; Diefendorf and Freimuth, 2017; Eglinton and Eglinton, 2008; Hemingway et al., 2016; Sachse et al., 2012). Although *n*-alkanes are a single class of compounds, they have the advantage of being derived from a number of different organisms, and often the number of carbons in the long-chain *n*-alkanes is diagnostic of the producing organism group. For example, aquatic algae predominantly produce the C_{17} *n*-alkane (Cranwell et al., 1987; Gelpi et al., 1970). Generally, the longer chain *n*-alkanes with chain lengths from 21 to 37 (C_{21} to C_{37}) carbon atoms are produced by higher plants and protect the leaf surfaces from desiccation and microbial degradation (Eglinton and Hamilton, 1967), although more recent studies show that the middle-chain *n*-alkanes (C_{23} and C_{25} *n*-alkanes) could originate from aquatic and semi-aquatic plants (Ficken et al., 2000) such as *Sphagnum* L. (Baas et al., 2000). These epicuticular leaf waxes are excellent biomarkers, because they are resistant to degradation, well preserved in the environment, and transported via aeolian and fluvial processes to sedimentary archives (Kawamura et al., 2003; Seki et al., 2010). Several studies have shown wide variations in the distribution of *n*-alkanes

among different spatial ranges (Dodd and Poveda, 2003) and plant types such as C3 and C4 plants (Diefendorf and Freimuth, 2017). C4 plants can exhibit longer *n*-alkane chains than C3 plants in some ecosystems (Diefendorf and Freimuth, 2017). However, the reconstruction of past C3 *vs* C4 biomass from leaf waxes must be performed from compound-specific carbon isotopes since C3 and C4 plants display different photosynthetic pathways, more efficient in the case of C4 plants, resulting in a ~10-15‰ $\delta^{13}C$ shift in the leaf waxes between both groups of plant endmembers (Tipple and Pagani, 2007). The carbon isotope fractionation of crassulacean acid metabolism (CAM) plants present an intermediate pattern between C3 and C4 plants, and thus their carbon isotope values overlap (O'Leary, 1988). The vegetation that covers the almost bare catchment basins of the Sierra Nevada alpine wetlands mainly consist of C3 plants. C4 plants are lacking from this alpine area (Garcia-Alix et al., 2017; Jiménez-Espejo et al., 2014; Jiménez-Moreno et al., 2013). The potential C4 plant contribution to the Holocene sedimentary records in the area is thus discarded, which simplifies the interpretation of the obtained *n*-alkane data.

Two indices are generally used to characterize the distribution of *n*-alkane chain lengths, the average chain length (ACL) and the carbon preference index (CPI). The ACL is the weighted average of odd-chained *n*-alkanes within a sample (Eq.1). ACL values can represent the response of the terrestrial plants to temperature (Kawamura et al., 2003; Vogts et al., 2009) and/or aridity (Calvo et al., 2004; Moossen et al., 2015; Zhou et al., 2005) with increasing values as temperature and aridity increase, as well as changes in vegetation. Nevertheless, temperature does not have a clear control on ACL throughout large geographical transects due to the specific ACL signature in different species (Diefendorf and Freimuth, 2017). Global ACL values have also been used in a wider geographical context to represent aeolian transport from different latitudinal belts showing changes in contributions from different source regions over large latitudinal gradients (Kawamura et al., 2003). Therefore, it is of paramount importance to identify the environmental meaning of the different *n*-alkane chains in a specific study area, especially in extreme environments, in order to correctly interpret their molecular signature in the sediments (Vonk and Gustafsson, 2009). In this way, a plant and soil survey conducted in the alpine areas of the Sierra Nevada (including the LdRS site) revealed that the length of the *n*-alkane chain can be used as a proxy for water availability in these extreme environments with shorter chain lengths pointing towards development of aquatic environments (Garcia-Alix et al., 2017).

Equation 1 (Schefuß et al., 2003b):

$$ACL = \frac{\sum(x_i * C_i)_n}{\sum(C_i)_n}$$

where, x_i represents the n-alkane of a given chain length and C_i represents the concentration of the n-alkane. In this paper the ACL between the C_{25} and C_{33} alkanes is calculated.

The CPI reflects the predominance of odd-chained *n*-alkanes over even-chained *n*-alkanes in a given sample (Eq. 2). It can be used to track the quality of the studied proxies, algal input, and the possible alteration from original biogenic source material (Killops and Killops, 2005; Kvenvolden, 1966). In this way, CPI values >2 reflect a terrestrial plant source and thermal immaturity of the sample, and values <2 should be viewed with caution as they can either indicate a non-terrestrial source or diagenetic alteration (microbial breakdown or thermal alteration) (Bush and McInerney, 2013; Killops and Killops, 2005).

Equation 2 (Bray and Evans, 1961):

$$CPI = \frac{1}{2}\left(\left(\frac{C_{25}+C_{27}+C_{29}+C_{31}+C_{33}}{C_{24}+C_{26}+C_{28}+C_{30}+C_{32}}\right)+\left(\frac{C_{25}+C_{27}}{C_{26}+C_{28}}\right)\right.$$

where, C_n represents the concentration of an n-alkane with a specific number (n) of carbon atoms in its chain.

Another *n*-alkane index is the P_{aq} index, or 'portion aquatic' (Eq. 3). This index shows the contribution of submerged/floating aquatic macrophyte input versus emergent and terrestrial plant input into the lake sediments (Ficken et al., 2000). High P_{aq} values indicate high aquatic input and low values indicate low aquatic input relative to terrestrial material. It has been used as proxy for water availability in the Sierra Nevada alpine region (Garcia-Alix et al., 2017).

Equation 3 (Ficken et al., 2000):

$P_{aq} = (C_{23}+C_{25})/(C_{23}+C_{25}+C_{29}+C_{31})$

where, C_n represents the concentration of an n-alkane with a specific number (n) of carbon atoms in its chain.

1.3 Compound-specific hydrogen isotopes as a hydrological proxy

The compound-specific deuterium-to-hydrogen ratio of terrestrial plant waxes (δD_{wax}: mainly C_{27} to C_{31} alkanes) and aquatic plants (δD_{aq}: mainly C_{23} to C_{25} alkanes) records the signal of the environmental source water used by these plants. Recent studies have shown that changes in the δD of the source water are highly correlated with changes in the *n*-alkane δD for both terrestrial and aquatic organisms (Sachse et al., 2012; Sachse et al., 2006). In addition, there is a strong relationship between source water and *n*-alkane δD values in lake-surface sediments across different climatic gradients worldwide (Hou et al., 2006; Sachse et al., 2012; Sachse et al., 2004). This is mainly attributed to the fundamental control of mean annual precipitation (δD_{MAP}) on δD leaf wax values, especially site-averaged hydrogen isotopes in *n*-alkanes, which show a strong positive correlation globally (Sachse et al., 2012; Sachse et al., 2004). In the case of the hydrogen isotopes of terrestrial *n*-alkanes, they can also track fluctuations in the amount of precipitation at mid-low latitudes (Tierney et al., 2017). Therefore, changes in the sedimentary δD_{wax} and δD_{aq} values through time can be used to infer changes in precipitation and evaporation on land and from lakes (Hou et al., 2006; Seki et al., 2011).

1.4 Long-chain diols as a proxy for past temperatures

Long-chain alkyl diols (LCDs) are a promising paleotemperature proxy. Similar to the well-established marine alkenone paleotemperature proxy (Brassell et al., 1986), the structure of the algal biomarker is related to the growth temperature of the producing algae. With LCDs, the chain length and position of the hydroxyl group along the long-chain C_{28} and C_{30} diols is dependent on temperature in marine environments (Rampen et al., 2012). These LCDs have been found in both lake and marine sediments. More recently Rampen et al. (2014) explored a temperature calibration for freshwater environments and found that diol distributions from lake sediments show correlations with environmental temperature obtained from another organic proxy, GDGTs. The calibration agrees with the culture results from known Eustigmatophyte diol-producers; however, this is a developing proxy and more data are needed to refine it.

Different LCD indices such as the long-chain diol index (LDI: Eq. 4) or the multiple linear regression analysis on LCD distributions have been tested as annual and/or seasonal temperature loggers in both freshwater and marine environments (García-Alix et al., 2020; Lattaud et al., 2018; Rampen et al., 2014; Rampen et al., 2012; Smith et al., 2013). The presence of LCDs in the LdRS sedimentary record allowed the assessment of these different indices as paleotemperature proxies for the Sierra Nevada alpine wetlands. The best fit was obtained between mean annual air temperature data of the last~100 years and the LDI record (Eq. 5). Nevertheless, since this was the first LCD temperature calibration approach in an alpine lake, the reference temperature

time-series (~100 years) used in the calibration might not accurately reflect cold extreme past temperatures in LdRS (e.g., during the Little Ice Age -LIA-). Therefore, temperatures reconstructed from LDI values lower than 0.1 could present higher uncertainties than the mean standard error of the calibration (±0.3ºC) (García-Alix et al., 2020).

In the marine environment there are a number of algal taxa producing LCD, including diatoms of the genus *Proboscia* Sundström (Sinninghe Damsté et al., 2003) and the unicellular phytoflagellate *Apedinella radians* (Lohmann) Campbell (Rampen et al., 2011), among others. Based on research at Lake Baikal, Shimokawara et al. (2010) speculated that the source of these compounds in lakes might be Eustigmatophyte algae, which was confirmed by Rampen et al. (2014) and Villanueva et al. (2014). However, these expected LCD-algae producers in freshwater environments have not previously been identified in the study site (Barea-Arco et al., 2001; Sánchez-Castillo, 1988). In addition, the distribution of the relative abundances of the different diol isomers in LdRS seems to differ from the diol signature observed in previous studies suggesting that other potential diol producers might have been the source of LCDs in this alpine lake (García-Alix et al., 2020). Therefore, the obtained calibration equation in LdRS is a region-specific calibration for local alpine environments in the Sierra Nevada or for other lakes with similar LCD distribution as LdRS (García-Alix et al., 2020). Ongoing seasonal lake monitoring program and gene sequencing analyses will help determining the specific diol source in LdRS and reducing the uncertainties of the current LCD-temperature calibration (García-Alix et al., 2020).

Equation 4 (Rampen et al., 2012):

$$LDI = \frac{F_{C_{30}1,15-diol}}{F_{C_{28}1,13-diol} + F_{C_{30}1,13-diol}}$$

where the LDI (Long-chain Diol Index) is defined as the fractional abundance of the C_{30} 1,15-diol (m/z 341) relative to the combined fractional abundance of C_{28} 1,13- (m/z 313), C_{30} 1,13- (m/z 313), and C_{30} 1,15-diol (m/z 341).

Equation 5 (García-Alix et al., 2020):

MAAT (ºC) = 9.147 x LDI - 0.243 *mean standard error*=±0.28ºC

where, MAAT (ºC) and LDI represent Mean Annual Air Temperatures and the row long-chain diol index values, respectively.

2. Materials and Methods

2.1 Sedimentary record

Two adjacent sediment cores were collected in September 2006 at LdRS. Core 06-01 measured 1.5 m and was collected in the deepest part of the basin using a Livingstone corer. Core 06-02 was 0.37 m long and was taken with a universal short-corer. The bottom section of the core 06-01 contains mica schist gravels, and glacial clays, silts and sands. From 133 to 75 cm the record consists of organic sediments without obvious laminations. The rest of the core mainly consists of laminated organic clays and bryophyte layers. The chronology used here is constrained by ^{210}Pb, ^{137}Cs, and radiocarbon dates (Anderson et al., 2011). The age model was performed by means of Heegaard et al. (2005) R-based package for mixed-effect models. It provided an extrapolated age of ~12,300 cal. yr BP for the core bottom. The sedimentation rate varies from 0.007 cm/yr in the deepest part of the core to 0.13 cm/yr at the water-sediment interface (Anderson et al., 2011). The relationship between core depths and ages of the different organic and inorganic proxies published up to now from LdRS record can be found in García-Alix et al. (2018). Pollen, charcoal, carbon and nitrogen isotopes, major elements and trace elements were previously analysed from the same LdRS record (Anderson et al., 2011; García-Alix et al., 2018; Garcia-Alix et al., 2013; Jiménez-Espejo et al., 2014). In addition, the last 1500 years of the LdRS record were recently analysed for long-chain diols (García-Alix et al., 2020). All these data are compared to the results shown in this study

It has already been 9 years since the Anderson et al. (2011) study was published and radiocarbon calibration curves and software for age-depth modelling have been updated. In order to validate the chronology published in (Anderson et al., 2011), the ^{14}C ages, originally calibrated using the Intcal 09.14c calibration curve (Reimer et al., 2013), have been re-calibrated by means of the most recent calibration curve: the Intcal 13.14c curve (Reimer et al., 2013). The comparison of both calibrated datasets shows no difference between them (Table S1). In addition, the age model used in Anderson et al. (2011) have been compared with a new Bayesian age-model calculated by means of the R-based Bacon package, version 2.3.9.1 - July 2019 - (Blaauw and Christen, 2011) (see supplementary Fig. S1 for further information). Both age models are very similar, showing the same sedimentary rates with a maximum discrepancy of ~300 years at ~3500 cal. yr BP, probably due to different smoothing parameters between them (Fig. S1a). The uncertainties at 95% between both models share the same trend and agree in most part of the record (Fig. S1b). However, uncertainties of the model from Anderson et al. (2011) are higher than the proposed Bayesian approach. In this study we thus maintain the original LdRS age-model from Anderson et al. (2011),

considering that the discrepancies between both models are very small and therefore negligible. This also permits us to preserve the coherence with previously published studies from this record.

In this paper we follow the INTIMATE subdivision for the Holocene linked to a Global Stratotype Section and Point (GSSP) (Walker et al., 2012): early–middle Holocene boundary at 8200 cal. yr BP and a middle–late Holocene boundary at 4200 cal. yr BP.

2.2 Biomarker extraction, separation, and isotope analysis

A total of 102 sediment samples were taken at different intervals (ranging from 1 to 2 cm) throughout both LdRS 06-01 and 06-02 cores for *n*-alkane and hydrogen isotope analyses. The total lipids from freeze-dried and homogenised samples were extracted by ultrasonication using a dichloromethane/methanol mixture (3:1 v/v). Subsequently acids were separated from neutral compounds using aminopropyl-silica gel column chromatography after Toney et al. (2010). The neutral fraction was separated further using silica-gel chromatography after Moossen et al. (2013). The *n*-alkanes were analysed using a GC-FID (Shimadzu 2010) and a GC-MS (Shimadzu QP2010-Plus Mass Spectrometer interfaced with a Shimadzu 2010 GC). The instrument parameters and methods are identical to those described in Moossen et al. (2013) using a BP1 (SGE Analytical Science) column (60m, diameter: 0.25 mm, film thickness: 0.25 µm; coating: 100% Dimethyl-polysiloxane) using an injection standard of methyl behenate (100µg/ml) added to each sample. The *n*-alkanes were quantified by comparing their peak areas with the peak areas of the injection standard. The mean analytical error (mean standard deviation) of the analyses was determined by analysing 10 *n*-alkane containing fractions in duplicate. The analytical error (1 sigma standard deviation) associated with the quantification of the *n*-alkanes is ±4%, and that associated with the $CPI_{25\text{-}33}$, $ACL_{35\text{-}33}$, and P_{aq} ratios is 0.01, 0.02, and 0.001, respectively.

Hydrogen isotopic composition of sedimentary *n*-alkanes was measured with GC-IRMS. Compound-specific δD values of long-chain *n*-alkanes were measured using a GC-thermal conversion-IRMS system consisting of a HP 6890 GC connected to a Finnigan MAT delta Plus XL mass spectrometer. Thermal conversion of *n*-alkane to H_2 was achieved at 1450˚C in a microvolume ceramic tube. Analytical accuracy of the laboratory standard was within 5‰. In duplicate analyses of samples, standard deviations for *n*-alkane δD were usually better than 5‰. δD values are given in ‰ notation relative to the Vienna Standard Mean Ocean Water (VSMOW). C_{20} *n*-fatty acid methyl ester whose isotopic values were known was co-injected with the samples as an internal isotopic standard for δD measurements of *n*-alkanes.

3. Results

3.1 n-Alkane distributions

In general, the *n*-alkane stratigraphy from the LdRS record can be summarized as follows: the C_{29} and C_{31} *n*-alkanes are the most abundant from the bottom of the record (~12,280 cal. yr BP) to ~10,000 cal. yr BP. C_{27} dominates the *n*-alkane profile from ~10,000 cal. yr BP to 5770 cal. yr BP. Afterwards, the profile changes and C_{29} predominates again in the youngest part of the record.

The total *n*-alkane concentrations have been calculated in both units μg $gsed^{-1}$ and μg gOC^{-1} (Figs. 2a and 3a). Nevertheless, their general trends follow a similar pattern and we are only going to focus on the first one. The total *n*-alkane concentration in the studied samples (from C_{19} to C_{35}) ranges from 2.4 to 238.2 μg $gsed^{-1}$ with an average of 106.5 μg $gsed^{-1}$. *n*-Alkane concentrations remain below 16.0 μg $gsed^{-1}$ until ~10,350 cal. yr BP and then rise rapidly, peaking at ~8870 cal. yr BP (223.1 μg $gsed^{-1}$). This peak subsides quickly and values are maintained ~150 μg $gsed^{-1}$ until a step-wise increase at ~7170 cal. yr BP (238.2 μg $gsed^{-1}$) that is sustained until ~5400 cal. yr BP (193.9 μg $gsed^{-1}$). After this, concentrations remain relatively constant ranging between 80.5 and 149.3 μg $gsed^{-1}$ with minima at ~3170 and ~2040 cal. yr BP (20.5 and 45.0 μg $gsed^{-1}$, respectively). After ~260 cal. yr BP, the *n*-alkane concentration drops below 24.5 μg $gsed^{-1}$. These low values prevail through to present (Fig. 2a and 3a).

ACL values range from 28.1 to 29.3 with an average of 28.7±0.2. ACL values during the earliest part of the record are highly variable, but decline reaching 28.4, the lowest value of the early Holocene, at ~11,300 cal. yr BP. ACL values are high in the early Holocene from ~10,500 (28.8) until ~8350 cal. yr BP (28.8) and gradually decline down to 28.3 at ~6270 cal. yr BP, reaching the minimum value for the middle Holocene. A notable minimum occurs around 7430 cal. yr BP, with values close to 28.3. After ~6270 cal. yr BP, ACL values increase linearly toward the 18^{th} century with high superimposed variability and particularly high values from ~3170 to 2740 cal. yr BP (>29.1), at ~2040 cal. yr BP (29.1), ~1020 cal. yr BP (29.1), and ~260 cal. yr BP (29.3). A decreasing trend in ACL values can be observed from this date to the present, and it reached a minimum value ~70 years ago (28.3) (Fig. 2b and 3b).

The P_{aq} values range from 0.25 to 0.48 with an average value of 0.37±0.05. High P_{aq} values are consistent throughout the early Holocene from ~11,800 to

10,500 cal. yr BP. After a minimum value around 9300 cal. yr BP (0.34), an increasing trend can be recognized until ~6300 cal. yr BP (0.47). After ~6300 cal. yr BP, P_{aq} declines linearly until ~260 cal. yr BP (0.29). A rapid increase in the P_{aq} is detected in the last ~160 years of the record, reaching values of 0.47 (Fig. 2c and 3c). P_{aq} and ACL are inversely correlated (r=-0.87, p<0.0001, n=70).

The CPI values in the study sedimentary record range from 2.8 to 4.7, with an average of 3.9±0.4. CPI values are highly variable before ~11,000 cal. yr BP, falling below 3.0 from ~11,540 to 11,290 cal. yr BP. CPI values rise steadily until ~10,350 cal. yr BP and then remain stable with a gradual trend toward lower values. Notably lower CPI values occur from ~5590 to 4140 cal. yr BP and around 740, 110, and 20 cal. yr BP, with values close to 3.5 (Figure 2d and 3d).

3.2 n-alkane hydrogen isotopic values: δD_{wax} and δD_{aq}

A mean value of δD varied via chain length (C_{23} -177±12‰, C_{25} -173±16‰, C_{27} -178±16‰, C_{29} -178±12‰, C_{31} -182±10‰, C_{33} -185±12‰) and -179±14‰ for all *n*-alkanes throughout the record. The δD data from odd-chain *n*-alkanes all show similar overall trends and are significantly correlated (r from 0.64 to 0.93, p<0.0001, n from 52 to 68) (Table 1). However, δD values from terrestrial and aquatic/semiaquatic *n*-alkanes show differences on smaller time scales. There is a high correlation between δD values from the C_{29} to C_{33} of terrestrial plant leaf waxes (r from 0.84 to 0.93, p<0.0001, n from 57 to 68), being especially high between C_{29} and C_{31} (r= 0.93, p<0.0001, n=68). The δD values of the aquatic/semiaquatic plant leaf waxes, C_{23} and C_{25}, are also highly correlated (r= 0.85, p<0.0001, n=52). The C_{27} shares trends with both groups (Table 1). Thus, we categorize the δD values into two main groups: δD values of C_{29} and C_{31}, hereafter referred to as δD_{wax}, and δD values of C_{23} and C_{25}, hereafter referred to as δD_{aq} (Fig. 2g,h and 3g,h). Although there are similar trends between δD_{aq} and δD_{wax} values, oscillations are not always similar in both proxies. Both δD_{aq} and δD_{wax} have maximum values in the earliest part of the record before ~10,500 cal. yr BP (Fig. 2g,h) from -162‰ to -126‰ and from -168‰ to -146‰, respectively. The overall trend is toward lower δD_{aq} and δD_{wax} from the earliest Holocene to the middle Holocene with the minimum values of δD_{wax} at ~7170 cal. yr BP (-197‰), and the lowest values of δD_{aq} recorded between ~6270 and 5920 cal. yr BP (-199‰). However, an increasing trend can be recognized earlier in δD_{wax} values, starting around ~7100 cal. yr BP, which is delayed in δD_{aq} until ~5900 cal. yr BP (Fig. 2 g,h). In the late Holocene, a slight change toward more negative values started ~1800 years earlier in δD_{wax} (~3800 cal. yr BP) than in δD_{aq} (~2050 cal. yr BP). During the last ~500 years there is an abrupt decrease in

δD_{aq} that can be observed ~180 years later in the δD_{wax} (Fig. 2g,h and 3g,h). In general terms, the variability in the δD_{aq} values for the late Holocene (~44‰) is larger than those of δD_{wax} (~24‰).

Average δD_{aq} values are slightly higher than δD_{wax} ones throughout the record with mean δD_{aq} and δD_{wax} values of -173±16‰ and -180±11‰, respectively. Nevertheless, there are a few periods when the δD_{aq} values are lower than δD_{wax} values (e.g. from ~7000 to 5800 cal. yr BP; at ~4500, ~4000, ~260, and ~50 cal. yr BP). To facilitate this contrast, we calculate an index of δD_{wax} minus δD_{aq} (ΔD_{wax-aq}: Fig. 2f and 3f). Values above zero represent times when δD_{wax} is less negative than δD_{aq} and values below zero occur when δD_{wax} is more negative than δD_{aq}.

3.3 Long-chain diol Index fluctuations

Previously published LDI data of LdRS record for the last ~1500 years (García-Alix et al., 2020) are also included in the results and discussion in order to show a big picture of the variation of this proxy throughout the Holocene. LDI values range from 0.05 to 0.31 with an average value of 0.18±0.5. The LDI values hover around the mean throughout most of the Holocene with notably higher LDI values, from ~5000 to 4200 cal. yr BP, ~2540, ~1020, and after -10 cal. yr BP. Only a few notable LDI value declines occurred at ~6560, ~6170, and from ~4100 to 3900 cal. yr BP. However, the largest ones were recorded between ~450 and 150 cal. yr BP as well as between ~40 and 30 cal. yr BP (Figure 2e and 3e). LDI values were only in the same range as at present at around 4800-4650 cal. yr BP.

4. Discussion

4.1 The source of n-alkanes in Laguna de Río Seco during the Holocene

n-Alkane compounds in lacustrine records can be sourced in the local catchment or from long-distances, as allochthonous *n*-alkanes can be transported to lakes via aeolian or fluvial processes (Kawamura et al., 2003; Seki et al., 2010). In the Sierra Nevada, one long-distance source that needs to be considered is Saharan dust from North Africa, since Saharan dust episodes have been described in Sierra Nevada in both historical records after ~7100 cal. yr BP (Garcia-Alix et al., 2017; Jiménez et al., 2018; Jiménez-Espejo et al., 2014) and recent atmospheric deposition (Morales-Baquero et al., 1999). Here we use several lines of evidence to determine whether the sedimentary *n*-alkanes in LdRS are derived from Saharan dust or locally sourced.

Modern vegetation samples from LdRS catchment have mean ACL values ranging from 30.2±1.0 to 28.7±0.5, depending on their proximity to the water source (Garcia-Alix et al., 2017). The predominance of shorter carbon chains, and thus, the lowest ACL values come from plants growing in the flooding areas around the main water pools, such as Cyperaceae, Ranunculaceae, bryophytes, and graminoids (ACL values lower than 29); whereas larger ACL values correspond to local plants in the catchment basin, but further away from the main water pools (Garcia-Alix et al., 2017). Longer *n*-alkane chains, mainly C_{31} and less frequently C_{29} carbon chains, are usually the dominant *n*-alkanes in Saharan dust (ACL values between 29 and 30) (Eglinton et al., 2002; Huang et al., 2000; Schefuß et al., 2003a). Although at their uppermost range of ACL values at LdRS may overlap with the general Saharan dust ACL signal, these values most likely represent a predominantly local source. In addition, Holocene ACL and P_{aq} values in LdRS are consistent with aridity changes inferred from the local pollen record throughout the Holocene (Fig. 2b,c,4a) (Anderson et al., 2011). This is also in agreement with previous geochemical studies (Garcia-Alix et al., 2017; García-Alix et al., 2012b; Jiménez-Espejo et al., 2014) that suggested that the main sources of organic matter in the Holocene sedimentary record of alpine lakes and wetlands in this region were algae and plants from the catchment basin. In particular, these studies did not find evidence of carbon isotopic enrichment in the Holocene organic matter record of Sierra Nevada that would be derived from North African plant inputs (Fig. 4c) (Garcia-Alix et al., 2017; García-Alix et al., 2012b; Jiménez-Espejo et al., 2014). Future analyses of carbon isotopes in the longer *n*-alkane chains should corroborate this previous observation based on carbon isotopes of bulk organic matter. Finally, sedimentary δD_{wax} values for African derived *n*-alkanes in marine environments adjacent to the African continent showed that during the Holocene the δD_{wax} values of North and West African derived *n*-alkanes were greater than ~-160‰ (Collins et al., 2013; Niedermeyer et al., 2016; Niedermeyer et al., 2010). δD_{wax} values from sedimentary *n*-alkanes in LdRS are consistently lower than the African values, with a mean value of -180±11‰. Values are slightly higher than -170‰ before 10,500 cal. yr BP (Fig. 4m), and are coeval with the highest bulk organic $\delta^{13}C$ values (Fig. 4c) and relatively high Z/Th data (Fig. 4d) in the LdRS record. The low δD_{wax} values along with the strong similarity in long-term and short-term trends between δD_{aq} and δD_{wax} (r=0.79, p<0.0001 n=66) suggest that the predominant *n*-alkane signal at LdRS is from the local environment with perhaps an exception for *n*-alkanes deposited prior to ~10,500 cal. yr BP (see discussion below).

Although the aeolian aerosol deposition from North Africa does not appear to produce a direct input of *n*-alkanes into LdRS during the Holocene, there is an influence of the inorganic dust on the biogeochemistry and productivity in this

oligo-mesotrophic alpine lake. Previous studies showed that at present this aeolian input contributes with allochthonous nutrients such as nitrogen or phosphorous (Mladenov et al., 2011; Pulido-Villena et al., 2005; Reche et al., 2009), which were also likely to be a significant source of nutrients in the past to LdRS (Garcia-Alix et al., 2017; Jiménez-Espejo et al., 2014). The reason for the absence of evidence for North African sourced organic matter in the sedimentary record might be due to the higher input of locally sourced organics in the record.

4.2 Long-chain diol-inferred temperature in LdRS

The LDI-inferred temperatures using Equation 5 (García-Alix et al., 2020) show that MAAT fluctuated by ~2.4ºC during the Holocene. However, the reconstructed temperatures should be taken with caution considering the low range of the reconstructed MAAT and the mean standard error of the applied calibration (±0.28ºC). In general, the average mean annual air temperature anomalies (MAATA respect to the reference period 1979-2008 of the Common Era -CE-) during the Holocene was 1.0±0.4ºC lower than that of the reference period. MAATA closely oscillated around this mean value, especially during the early-middle Holocene; however, abrupt temperature changes occurred during the middle-to-late Holocene transition.

Estimated temperatures were notably high from ~5000 to 4200 cal. yr BP, and surprisingly, from ~4800 to 4650 cal. yr BP, under a non-anthropogenic scenario, temperatures were as high as in the present global warming scenario, recording positive MAATAs. Marine temperature records also show a warm period from ~5000 to 4200 cal. yr BP in both western (Cacho et al., 1999; Martrat et al., 2004; Rodrigo-Gámiz et al., 2014) and eastern (Castañeda et al., 2010) (Fig. 4e-i) Mediterranean regions. These temperatures were also higher than the ones during the Medieval Climate Anomaly (MCA). This warm period in the middle Holocene ended abruptly at around 4150-4100 cal. yr BP, reaching a minimum MAATA at ~4000 (-1.5ºC). Late Holocene temperatures in LdRS continued oscillating around the average MAATA until ~1020 cal. yr BP, during the MCA, when MAATA increased sharply to -0.5ºC, as in the western Mediterranean region (Moreno et al., 2012). Subsequently, temperatures dropped during the LIA reaching the lowest value of the record at ~260 cal. yr BP (-2.2ºC MAATA). Temperature has since increased until present, except for a sharp and short decline at the beginning of the 20th century (-1.7ºC MAATA). Temperature trends during the 20th century match the global consensus view of changes occurring due to the current global warming scenario (García-Alix et al., 2020; IPCC, 2013).

4.3 Application of the δD_{wax} and δD_{aq} to past hydrology at LdRS

The primary control on the hydrogen isotopic signature of leaf waxes comes from the leaf water, which depends on the source water that plants capture from the soil (terrestrial plants) or water bodies (aquatic/semiaquatic plants) that ultimately comes from the precipitation or groundwater supply (see Sachse et al. (2012) for an extensive review of this topic). The studied sedimentary *n*-alkanes in LdRS are derived from local aquatic and catchment terrestrial plants. They would track the average δD composition of their source water and thus, the hydrological changes within LdRS (affected by evaporative processes) and the surrounding terrestrial system (affected by plant evapotranspiration processes). δD_{aq} and δD_{wax} records show similar trends suggesting that they share common source water, namely meteoric water that recharges soil and lake waters. Nevertheless, these parallel trends could also reflect the balance between lake evaporation *vs* terrestrial plant evapotranspiration (see discussion below).

Meteoric water at LdRS mainly occurs as snow precipitation, which recharges the lake and soil moisture during annual melt. In the case of southern Iberia, the isotopic composition of precipitation is primarily influenced by the MAAT (positive correlation) (García-Alix, 2015), the amount of precipitation, and the water vapour source (Araguas-Araguas and Diaz Teijeiro, 2005). Therefore, precipitation source, precipitation amount, and temperature likely influence their signal and reinforce each other, as also occurs in central and northern Europe (Sachse et al., 2004). There are no long-term data series of hydrogen isotopic composition in precipitation at high elevation in the Sierra Nevada. Only occasional data from four winter precipitation events (snow) between 2001 and 2003 CE provided average δD values around -121±4‰, -117±10‰, -107±14‰, and -99±3‰ (Raya Garrido, 2003). These data from occasional precipitation events are slightly lower than the modelled δD values by means of the OIPC - Online Isotopes in Precipitation Calculator - (Bowen, 2020) for the cold season precipitation in LdRS (δD= -91±2‰). The average modelled precipitation δD for the warm season was -37±2‰, and the mean annual weighted values range from -78 to -65±2‰ (Bowen, 2020). This mean annual weighted isotopic composition of precipitation in LdRS mainly registers the snow precipitation from October to May, since rainfall is rare at such high elevation and primarily occurs from June to September, which are also the driest months (Spanish National Weather Agency - AEMet Open Data, 2020). All these precipitation data are in the range of the expected precipitation δD in the south of the Iberian Peninsula (Fig. 5). These mean annual δD values of precipitation in LdRS also agree with the range of the calculated δD source water from the most recent *n*-alkane samples (40 and 60 years ago), after applying the general mean hydrogen isotope fractionation constant between *n*-alkanes and meteoric water: $\varepsilon_{C23/w}$, $\varepsilon_{C25/w}$, $\varepsilon_{C29/w}$, and $\varepsilon_{C31/w}$, respectively

747 (Sachse et al., 2004). The obtained δD water values range from -70‰ to -
748 55‰ for C_{31} and C_{29} *n*-alkanes, and from -63‰ to -25‰ for C_{23} and C_{25} *n*-
749 alkanes. The values from C_{29} and C_{31} *n*-alkanes (mainly form terrestrial
750 plants) are within the expected range of precipitation δD in LdRS; however,
751 the ones from C_{23} and C_{25} (mainly form aquatic and semiaquatic plants),
752 although partially agree with the δD values of meteoric waters, it seems that
753 they are more influenced by evaporative processes of lake waters.
754
755 Two main precipitation moisture sources have been observed in the
756 Mediterranean side of southern Iberia, including LdRS. The majority of the
757 precipitation mainly occurs in the cold season and is related to the westerlies
758 that bring (north and tropical) Atlantic moisture with a low δD signature.
759 However, this area is also influenced by Mediterranean vapour-water air
760 masses that carry a high δD signature, especially during the warm season
761 (Fig. 5) (Araguas-Araguas and Diaz Teijeiro, 2005; Esteban-Parra et al.,
762 1998; Gimeno et al., 2010; Oliva and Moreno, 2008). Similar precipitation and
763 isotopic patterns have been described in other parts of the Iberian Peninsula
764 (Krklec and Domínguez-Villar, 2014; Moreno et al., 2014) and western
765 Mediterranean areas (Celle-Jeanton et al., 2001). Occasional, isotopically-
766 depleted moisture coming from high latitudes such as northern Europe,
767 Russia or Arctic areas have a minor contribution to the annual precipitation in
768 the Iberian Peninsula, and thus to its mean weighted isotopic composition
769 (Araguas-Araguas and Diaz Teijeiro, 2005).
770
771 δD_{aq} and δD_{wax} data in LdRS show high deuterium values during the latest
772 Pleistocene-Holocene transition, low values during the early Holocene and
773 part of the middle Holocene (10,500-6000 cal. yr BP) and high values again
774 during the middle-late Holocene. They are consistent with the humidity trends
775 observed in the Sierra Nevada area at both high and low elevation that show
776 that precipitation was higher in the early-middle Holocene than during the late
777 Holocene (Anderson et al., 2011; García-Alix et al., 2017; Jiménez-Espejo et
778 al., 2014; Ramos-Román et al., 2018). In this regard, the potential isotopic
779 effect of the different types of precipitation (snow *vs* rain) related to different
780 long-term climatic episodes (e.g., cold-humid *vs* warm-arid) on the LdRS
781 record has also to be assessed considering different aspects. Firstly, snow
782 usually occurs in the Sierra Nevada above 1000 masl, being mostly persistent
783 in the cold season above 2000 masl (Pérez-Palazón et al., 2018). Secondly,
784 the mean annual weighted isotopic composition of precipitation in LdRS at
785 3020 masl mainly registers the signal of the snow precipitation during the
786 present warmest and driest period in the Holocene history of LdRS.
787 Therefore, past wetter and/or colder periods in LdRS would have also been
788 registering snow precipitation for the most part of the year. As far as
789 temperature trends in LdRS are concerned, there is no positive long-term
790 relationship between *n*-alkane δD and LDI-derived temperatures in the

Holocene, indicating that there is no long-term influence of temperatures on the isotopic composition of meteoric waters in this alpine site.

Considering all mentioned above, long-term oscillations in *n*-alkane δD may be related to changes in both the isotopic composition of precipitation source and the amount of precipitation (aridity *vs* humidity) in the western Mediterranean. All in all, the overall low D_{aq} and δD_{wax} values recorded during the early to middle Holocene in agreement with more humid conditions (Fig 4a,m) would also suggest a major Atlantic source of precipitation. The increase in both δD signals after ~6000 cal. yr BP suggests that Mediterranean sourced precipitation then became more frequent at this site, coevally with enhanced arid conditions (Fig. 4a,m,n, Fig. 5). The studied *n*-alkane δD records suggest that the influence of the Mediterranean precipitation in southern Iberia might have been enhanced by either the general low impact of Atlantic westerlies during the middle-late Holocene (reducing winter precipitation under a prevailing long-term NAO positive mode) (Olsen et al., 2012), and/or the establishment of the current Mediterranean dynamics (e.g., WeMO) after ~6000 cal. yr BP.

In addition to the overall trends that point to shifts in the source and amount of precipitation, some differences occur between δD_{aq} and δD_{wax} values that suggest there are smaller-scale and potentially locally driven changes that alter the recorded δD values within the terrestrial versus aquatic systems. For example, δD_{aq} is subjected to the controls on δD of the lake water, such as precipitation, residence time, evaporation, and even salinity (Aichner et al., 2017; Jacob et al., 2007; Leng and Marshall, 2004; Rach et al., 2017). Evaporation has a strong control on LdRS lake level, which varies by as much as 1.3 m on an annual basis (Anderson et al., 2011). In contrast, δD_{wax} values are mainly driven by precipitation and evapotranspiration by terrestrial plants, what is called "leaf water deuterium enrichment: Δ^2H_e" (Rach et al., 2017). Thus, despite possible offsets in biosynthetic fraction factors between aquatic and terrestrial plants (Rach et al., 2017; Sachse et al., 2004), the differences between δD_{wax} and δD_{aq} in LdRS should mainly be driven by evapotranspiration in the terrestrial system and lake evaporation in the aquatic system. In this line, Rach et al. (2017) proposed the use of Δ^2H_e ($\Delta D_{wax\text{-}aq}=\delta D_{wax}-\delta D_{aq}$) to express the isotopic difference between these two pools, which eventually register the ^2H enrichment of leaf water in terrestrial plants. Similarly, we use this difference, but adapted it to the alpine environment in order to highlight the differences in plant evapotranspiration versus lake evaporation. On average, δD_{aq} values are higher than δD_{wax} ones, which represent greater evaporation off the lake surface than evapotranspiration from terrestrial plants throughout most of the Holocene, but for two main

occasional episodes of environmental instability. $\Delta D_{wax\text{-}aq}$ is discussed in further detail below.

4.4 The latest Pleistocene-Holocene transition

The Pleistocene-Holocene transition is not often recognised in continental records from southern Spain. This period is particularly poorly represented in Sierra Nevada alpine environments, because glacial activity during the Younger Dryas (YD) eroded and covered previous glacial sedimentary basins with sand and gravel (Palade et al., 2011). The LdRS record is the only record to date that extends into this transition. Little is known from this period at LdRS due to the low organic and pollen concentrations (Anderson et al., 2011; Jiménez-Espejo et al., 2014). Although we were able to extract biomarkers from these early sediments, the results are interpreted with caution, first, because there are no dates in this interval and the only way of getting an age inference is by extrapolation; secondly, the concentrations of the *n*-alkanes are low (<16 μg $gsed^{-1}$; most of the cases <10 μg $gsed^{-1}$) in the oldest samples of the record.

The earliest part of the record is older than ~10,500 cal. yr BP and possibly as old as ~12,300 cal. yr BP and the geochemical data appear to be different from the Holocene average for all of the organic geochemical proxies derived from the *n*-alkanes. Specifically, ACL values are relatively high; δD_{wax} and δD_{aq} values are higher than any other period in the Holocene, and CPI values are overall low, but variable (Fig. 2). Because this high alpine region was likely ice-covered in the latest-Pleistocene, these biomarkers could represent an assemblage of sediment from different ages that occurred during the ice-melt. For instance, if the drainage basin was partially deglaciated, inputs would include dust trapped in old ice that was melting - along with contemporary dust from lower elevations, and eroded sediments from the catchment. High concentrations of local *Artemisia* are also detected in the pollen record at this time suggesting that arid conditions prevailed (Anderson et al., 2011). The high Zr/Th ratios (Fig. 4d) and the bulk organic $\delta^{13}C$ data (Fig. 4c) prior to ~10,500 cal. yr BP (Jiménez-Espejo et al., 2014), together with the biomarker evidence would support a possible atmospheric deposition (Saharan/north African airborne dust) of allochthonous organic matter, probably as C4 plant in aerosols (high bulk organic $\delta^{13}C$ values, Fig. 4c). Therefore, the sparse ground cover by terrestrial herbs and shrubs before ~10,500 cal. yr BP may have allowed for the dominance of Saharan aeolian-derived *n*-alkane input either due to active early Holocene air masses, or via 'old carbon' stored in local rock and ice glaciers that were melting (Jiménez-Espejo et al., 2014). The chromatography of the *n*-alkanes and predominance of odd-over-even chains (CPI) suggest that despite a potentially long-distance

and/or 'old' source, the lipids are still intact with little degradation (Fig. 2d). In any case, the possibility of primary sedimentation exists, because both Oliva et al. (2014) and Palade et al. (2011) suggested that the Sierra Nevada was (perennially) ice-free as early as 15,000-14,000 cal. yr BP. In either case, the biomarkers from this interval could likely come from a mix of sources spatially and temporally. Both bulk organic $\delta^{13}C$ data (Jiménez-Espejo et al., 2014) and biomarkers do not support the hypothesis of input of North African organic matter after ~10,500 cal. yr BP (Fig. 4)(see Section 4.1).

ΔD_{wax-aq} fluctuate in this interval, but show the largest negative offset during the latest Pleistocene to early Holocene transition (~30‰). However, the potential mixed source of these inputs makes the cause of the offset difficult to determine. Meltwater would carry a low δD value agreeing with a decrease in both the deuterium values for δD_{wax} and δD_{aq} after ~10,500 cal. yr BP (Fig. 2g,h and Fig. 4m,n). The P_{aq} and C/N values suggest predominantly aquatic environments after ~10,500 cal. yr BP. The relatively high input of aquatic material relative to terrestrial plant material is consistent with the lack of soil development after the erosive phase of the latest Pleistocene and typical time lag between deglaciation and terrestrial plant establishment. For example, a similar lag in Iceland following deglaciation has been detected (Caseldine et al., 2003). The lithology of the LdRS sediment core corroborates a glacial origin of sediments prior to the 10,500 cal. yr BP with glacial sands and clays, as well as mica schist clasts (Anderson et al., 2011). The biomarker evidence parallel the predominance of the colonial green algae *Botryococcus* Kützing in the earliest part of the Holocene (Anderson et al., 2011). The CPI rises after ~11,000 cal. yr BP, which likely represents a mix of sources for the *n*-alkanes from a mainly aquatic source towards a terrestrial one after the reduction of ice and rock glaciers in Sierra Nevada around 10,500 cal. yr BP (Palade et al., 2011). This is supported by the rise and stabilization of *n*-alkane concentrations at this time.

4.5 Early-middle Holocene paleoenvironmental reconstruction of the LdRS catchment basin – 10,500 to 6500 cal. yr BP

In the early Holocene, the climate surrounding LdRS is characterized by wet conditions with the highest lake levels (Anderson et al., 2011; Jiménez-Espejo et al., 2014). The beginning of the Holocene is marked by the rise in *n*-alkanes concentrations after ~10,500 cal. yr BP probably due to enhancements of aquatic productivity, shown by a low C/N ratio (Fig. 4b) (Jiménez-Espejo et al., 2014), high-moderate P_{aq} (Fig. 2c), an increase in the $(C_{19}+C_{21})/(C_{19}+C_{21}+C_{29})$ ratio (not shown), and algae presence (e.g. *Botryococcus*) (Anderson et al., 2011), along with the expansion of the high-elevation terrestrial plant communities, related to moderate-high ACL values

(28.8-29.0) from 10,500 to 9600 cal. yr BP. These high ACL values in some ways are counterintuitive during this wet phase, but in agreement with the potential increase in terrestrial plant communities and with the Holocene summer insolation maxima (Laskar et al., 2004). These ACL values are in the range of the vegetation that grows within the lake and/or on the shore of alpine lakes in Sierra Nevada at present (Garcia-Alix et al., 2017), corroborating the presence of sedges, graminoids and bryophytes surrounding the lake (Anderson et al., 2011). ACL values decline starting at ~9300 cal. yr BP is coeval with especially high P_{aq} (>0.34) and low C/N ratios. This might indicate a significant occurrence of aquatic/subaquatic species until ~6500 cal. yr BP. Temperatures during this period are relatively constant from ~8900 cal. yr BP (when the LDI record starts) to ~6500 with a MAATA of -1.1±0.2ºC with respect to the reference period, suggesting that precipitation might have occurred mostly as snow. The maximum temperatures during this period occurred at ~7430 and 6720 cal. yr BP (MAATA = -0.7ºC), and the minimum at 6560 cal. yr BP (MAATA=-1.6ºC). Both δD_{aq} and δD_{wax} values remain low from 10,500 to 6500 cal. yr BP, which supports the wet climate at this time with high precipitation mainly sourced from the Atlantic Ocean. It is important to note that there are negative peaks in the ΔD_{wax-aq} that may indicate periods of high evaporative conditions likely driven by the high insolation. In particular, ΔD_{wax-aq} values are low at ~9550 and from ~8130 to 7170 cal. yr BP. The ACL, ΔD_{wax-aq}, and LDI-inferred temperatures taken together suggest that the environment surrounding LdRS experienced effects of high summer insolation and a slight warming during the early-middle Holocene.

4.6 Middle Holocene paleoenvironmental reconstruction of the LdRS catchment basin – 6500 to 4200 cal. yr BP

This is a transitional period in LdRS. Cool temperatures occurred within the lake from ~6300 to 5500 cal. yr BP. However, LDI data support a gradual warming, with some oscillations, after 6170 cal. yr BP. Temperature increase became more intense between ~5080 and 4700 cal. yr BP, shifting ~1.1ºC (note that the mean standard error of the LDI-temperature calibration is ±0.28ºC). This marked the beginning of the sustained mid-Holocene warm event (between ~5000 and 4200 cal. yr BP) that registered the highest middle Holocene MAATA, ranging from -0.4 to +0.2ºC, suggesting temperatures on par with modern warming.

Terrestrial input to the lake continued during the middle Holocene at LdRS as evidenced by gradual ACL increase, but the P_{aq} also infers changing proportions of aquatic material. Overall the P_{aq} values indicate a productive aquatic system until ~6300 cal. yr BP. However, P_{aq} values continually

decline, with oscillations, from ~6300 cal. yr BP to 4200 cal. yr BP (Fig. 2c) pointing towards a gradual reduction of the water availability in the catchment (Garcia-Alix et al., 2017), and therefore, a major shift from aquatically derived material to material derived from the terrestrial system. These trends in ACL and P_{aq} values are also supported by the increasing elemental C/N ratio at ~6000 cal. yr BP, and an increase in the aridity deduced by the Zr/Th ratio (Saharan dust inputs) (Fig. 2b,c and Fig. 4b,d) (Jiménez-Espejo et al., 2014).

This increase in terrestrial inputs during the final part of the middle Holocene is also observed in organic proxies (both bulk sediment and biomarkers) of the neighbouring peatlands Borreguil de la Virgen -BdlV- (Garcia-Alix et al., 2017; García-Alix et al., 2012b) and Borreguil de la Caldera -BdlC- (Garcia-Alix et al., 2017). The maximum development of these peatlands coincides with the longest period of sustained warming in the diol record from ~5000 to 4200 cal. yr BP mentioned above. Wetland and some subaquatic plants occurred with abundances higher than 10% prior to ~5700 cal. yr BP in LdRS (Anderson et al., 2011), but it appears that the warming after this time had significant effects on the lake ecosystem, as well as, the surrounding terrestrial vegetation. The occurrence of submerged aquatic macrophytes, for example, is scarce in the palynological record at this time with only sparse amounts of pollen of the submerged plant *Potamogeton* L. (Anderson et al., 2011). In particular, the onset of warming coincides with a middle Holocene peak in *Pinus* L. pollen percentage and subsequent decline (Anderson et al., 2011) (Fig. 4a).

This transitional period, and more specifically from ~6500 to 5500 cal. yr BP, is a phase of environmental instability. This phase is coeval with the end of the African Humid Period in the western Mediterranean area (deMenocal et al., 2000), as well as, with a change in the westerly wind dynamics and shifts in the solar and oceanic influence (Fletcher et al., 2013). While isotopically-depleted precipitation from the North Atlantic region dominated during the early-middle Holocene, occasional, isotopically-enriched precipitation from the Mediterranean water masses became important during the middle-late Holocene in LdRS. There is also a change in ΔD_{wax-aq} values that appear to record an abrupt event from ~6300 to 6000 cal. yr BP (Fig. 4l) related to a change in the hydrology of the catchment, which is also in agreement with an abrupt shift in the C/N ratio of the bulk organic matter (Fig. 4b) (Jiménez-Espejo et al., 2014). This instability phase means the end of an early-middle Holocene humid period (overall low δD values) and the beginning of an aridity trend in the middle-late Holocene (overall high δD values), which has been identified in a number of previous studies in the Sierra Nevada (Anderson et al., 2011; Garcia-Alix et al., 2017; García-Alix et al., 2012b; Jiménez-Espejo et al., 2014; Jiménez-Moreno and Anderson, 2012; Jiménez-Moreno et al.,

2013; Mesa-Fernández et al., 2018; Oliva et al., 2014), and throughout the western Mediterranean region (deMenocal et al., 2000) where there is a gradual forest decline (Combourieu Nebout et al., 2009).

The compound-specific H-isotopes of terrestrial and aquatic plant *n*-alkanes recorded a large positive offset in ΔD_{wax-aq} at ~6000 cal. yr BP (19‰), which is unusual, because on average the δD_{aq} values remain about 7±10‰ greater than the δD_{wax} values throughout the record. From ~6300 to 6000 cal. yr BP, δD_{aq} values decline to the lowest values in the downcore record, while the δD_{wax} values remain stable. This situation could be explained by: (1) the amount of low δD source water increased to the lake, such as an increase in the amount of meltwater to the lake from the surrounding cirque basin, and/or (2) the occurrence of especially cold-humid winter conditions that prevented the catchment from completely thawing and evaporating in the summer. The latter scenario would also prevent extensive terrestrial plant growth in the catchment and its subsequent deposition into the lake, as a large part of the terrestrial catchment basin would remain covered by snow or frozen throughout most of the year (enhanced winter conditions). This interpretation is supported by the low LDI-inferred temperatures indicating that there were sustained cold winter conditions from ~6300 to 6000 cal. yr BP (Fig. 4j), and thus reduced lake water evaporation. This is also in agreement with a drastic drop of the TOC content (low productivity)(Jiménez-Espejo et al., 2014), low C/N ratio (predominance of aquatic over terrestrial productivity) (Fig. 4b), high P_{aq} (Fig. 2c), and low Mg/Al ratio (scarce catchment erosion/runoff) at this time (Jiménez-Espejo et al., 2014). Important changes in the North Atlantic climate system occurred from ~6500 cal. yr BP to 5500 cal. yr BP, such as the change in the dynamics of the North Atlantic westerlies (Fletcher et al., 2013), that would have enhanced cold seasons in the Sierra Nevada during this period. LDI-temperatures show that this period ended with rapid and sustained warming in LdRS from ~5600 to 4200 cal. yr BP, as sea surface temperatures in the western and eastern Mediterranean realm (Cacho et al., 1999; Castañeda et al., 2010; Rodrigo-Gámiz et al., 2014) (Fig. 4 e-i). The rapid temperature rise in LdRS, reaching warmer temperatures than the early Holocene, was likely strengthened by the lack of buffering by meltwater once the year-on-year snowpack was reduced (e.g., less precipitation under prevailing NAO positive conditions (Olsen et al., 2012)) and permanent glacial ice disappeared. This situation gave rise to the enhanced development of terrestrial vegetation in the catchment (ACL and C/N increase and P_{aq} decrease).

4.7 Late Holocene paleoenvironmental reconstruction of the LdRS catchment basin – 4200 cal. yr BP to present

In the late Holocene, the aridification trend continues, evidenced by ACL and P_{aq}, while the $\Delta D_{aq\text{-}wax}$ becomes more variable after ~4200 cal. yr BP. Three temperature minima were reached at ~4100-4000, 260, and 35 cal. yr BP, with -1.5, -2.2, and -1.7ºC MAATA, respectively. Three temperature maxima also occurred at ~2530 and 1020 cal. yr BP and present day, with -0.6, -0.5 and +0.2 ºC MAATA, respectively. Only the modern warming event has a temperature anomaly above the historical reference period (1979-2008 CE) during this phase. The warmest temperature prior to the modern period was reached during medieval times (-0.5 ºC MATA). Although P_{aq} and ACL show a small decrease in aquatic inputs, and less water availability, there was not important increase in evaporation at this time, according to the $\Delta D_{wax\text{-}aq}$ record.

$\Delta D_{wax\text{-}aq}$ shows strong peaks in evaporation at ~3000, 2040, 1400, 440 cal. yr BP, and 1960 CE. Those evaporation stages agree with a decrease in P_{aq} values, except at 1960 CE. The low P_{aq} values at ~3000, 2040, and 1400 cal. yr BP occurred at the same time as relatively high ACL values, supporting drier conditions.

As in the case of the instability phase between ~6500 and 5500 cal. yr BP, a rapid series of events in LdRS after ~500 cal. yr BP ended up with the melting of the frozen catchment basin, snowpack and permafrost that were built up during the LIA at LdRS. The evolution of the LIA in the Sierra Nevada follows the typical bi-modal pattern of the western Mediterranean (Nieto-Moreno et al., 2011). It started with a dry phase around 500 cal. yr BP under a moderate NAO positive mode (Trouet et al., 2009), which was coeval with cold temperatures (low LDI) and a large increase in δD_{aq} values (a considerable negative $\Delta D_{wax\text{-}aq}$ value: enhanced lake evaporation). Subsequently, very cold temperatures and humid conditions in LdRS occurred at ~260 cal. yr BP under a sharp NAO negative excursion (Trouet et al., 2009) (Fig. 4k) causing enhanced winter conditions that gave rise to significant snow and ice fields covering large parts of the LdRS catchment. The Mg/Al ratio and TOC values were also quite low during this event (Jiménez-Espejo et al., 2014), indicating decreased catchment erosion, as well as sparse plant cover. Snow and ice would have remained in the terrestrial catchment even during part of the summer, inhibiting extended terrestrial plant growth by delaying start of the growing season, and reducing the lake evaporation also affected by low temperatures. This situation would cause low δD_{aq} values, and thus largest positive offset in the $\Delta D_{wa\text{-}aq}$ record (20‰) at ~260 cal. yr BP (enhanced plant evapotranspiration or reduced lake evaporation), along with the minimum LDI-derived temperatures (-2.3ºC MAATA). However, this large δD_{aq} offset is only supported by one data point, and more data would be desirable to infer a clear shift. This observation would be consistent with the presence of two

important glacier fields above ~2900 masl in the Sierra Nevada from the 16th to the 20th century (Oliva et al., 2018). Although those glacier fields were located on the north face of the Sierra Nevada (Oliva et al., 2018), thick snow fields and permafrost should have developed in some high south-facing cirques during the LIA too. This would have been the case of Rio Seco cirque at ~3020 masl. Snow and ice accumulations in LdRS catchment melted gradually caused by the temperature increase after the LIA as well as the potential effect of other non-climatic environmental drivers (e.g. atmospheric dust and pollution deposition) (García-Alix et al., 2020). This melting was nearly complete in the first half of the 20th century (Oliva et al., 2014). As a result, the C/N ratio, *n*-alkane indices (increase in the P_{aq}, along with an abrupt drastic decline in ACL) and the general lower δD signature of *n*-alkanes point towards more water availability in the LdRS catchment, which is counterintuitive with the scarceness of rainfall in southern Iberian Peninsula at that time (Rodrigo et al., 1999) (Fig. 3i). Similar to the instability phase at ~6000 cal. yr BP, this transition finishes with the mentioned abrupt temperature rise after the ~1920s, reaching maximum MAATAs (0-+0.2ºC) at the top of the record (2003-2008CE). But contrarily to the instability phase at ~6000 cal. yr BP, in this modern case the system is amplified by anthropogenic forcing and has not returned to a steady state (García-Alix et al., 2020).

5. Concluding remarks

Major geochemical changes in algal and leaf wax lipids show three main phases of instability throughout the last ~12,000 years in alpine wetlands from the southern Iberian Peninsula: one that ended at ~10,500 cal. yr BP (latest Pleistocene-early Holocene), another from ~6500 to 5500 cal. yr BP (middle Holocene), and the last one after ~500 cal. yr BP (latest Holocene). Between these periods of abrupt changes, two periods that lasted between 4000 and 5000 years showed quite constant environmental conditions, at least in hydrology and evapotranspiration balance.

During the early-middle Holocene (from ~10,500 to 6500 cal. yr BP) an extensive development of alpine aquatic systems with high water levels predominated in the Sierra Nevada coevally with prevailing humid conditions. δD values also suggest that precipitation was mainly sourced in the Atlantic Ocean during this period. All the changes described in the middle Holocene instability phase (from ~6500 to 5500 cal. yr BP) gave rise to landscape changes in the Sierra Nevada, including a decrease in lake water levels and a development of peatlands from shallow lakes (Garcia-Alix et al., 2017a; García-Alix et al., 2012b). δD values, which agree with a decrease in precipitation after this transition, would indicate that even though precipitation

in southern Iberia was also sourced in the Atlantic Ocean during the middle-late Holocene, there was some Mediterranean moisture influence as well.

The main effect of temperature in these high elevation areas is the control on the length of the snow cover through the year, triggering or attenuating the thawing, and thus, the catchment snow-free surface. On the other hand, temperature rise can be amplified with respect to low elevation sites during dry and relatively warm periods (permafrost and snow cover decrease), as happened from ~5000 to 4200 cal. yr BP (especially from ~4800 to 4650 cal. yr BP) and at present. These are the only periods where temperature anomalies are positives in LdRS, reaching +0.2ºC. In the case of the last 100 years this amplification is also caused by anthropogenic forcing.

All these findings support the importance of the balance between temperature and hydrology in these endangered ecosystems, having an effect on the length of the snow-free season and the water availability throughout the year, and thus, impacting on the diversity and persistence of local alpine ecosystems.

Acknowledgements

This study was supported by the project P11-RNM-7332 of the “Junta de Andalucía”, the projects CGL2013-47038-R and CGL-2017-85415-R of the “Ministerio de Economía y Competitividad of Spain and Fondo Europeo de Desarrollo Regional FEDER” and the research group RNM0190 (Junta de Andalucía). A.G.-A. was also supported by a Marie Curie Intra-European Fellowship of the 7th Framework Programme for Research, Technological Development and Demonstration of the European Commission (NAOSIPUK. Grant Number: PIEF-GA-2012-623027) and by a Ramón y Cajal Fellowship RYC-2015-18966 of the Spanish Government (Ministerio de Economía y Competividad). J.L.T. was also supported by a Small Research Grant by the Carnegie Trust for the Universities of Scotland and hosted the NAOSIPUK project (PIEF-GA-2012-623027). We also want to thank the Editor, P. Rioual and two anonymous reviewers for their useful comments that improved the final version of the manuscript.

Appendix A. Supplementary data

Supplementary data to this article can be found online at https://www.journals.elsevier.com/quaternary-science-reviews

Research data for this article

Research data for this article can be found online at PANGAEA website.

References

Aichner, B., Hilt, S., Périllon, C., Gillefalk, M., Sachse, D., 2017. Biosynthetic hydrogen isotopic fractionation factors during lipid synthesis in submerged aquatic macrophytes: Effect of groundwater discharge and salinity. Organic Geochemistry 113, 10-16.

Alonso-González, E., López-Moreno, J.I., Navarro-Serrano, F.M., Revuelto, J., 2020. Impact of North Atlantic Oscillation on the Snowpack in Iberian Peninsula Mountains. Water 12, 105.

Álvarez-Lao, D., Kahlke, R.D., García, N., Mol, D., 2009. The Padul mammoth finds — On the southernmost record of *Mammuthus primigenius* in Europe and its southern spread during the Late Pleistocene. Palaeogeography Palaeoclimatology Palaeoecology 278, 57–70.

Ambaum, M.H.P., Hoskins, B.J., Stephenson, D.B., 2001. Arctic Oscillation or North Atlantic Oscillation? Journal of Climate 14, 3495-3507.

Anderson, R.S., Jiménez-Moreno, G., Carrión, J., Pérez-Martinez, C., 2011. Postglacial history of alpine vegetation, fire, and climate from Laguna de Río Seco, Sierra Nevada, southern Spain. Quaternary Science Reviews 30, 1615–1629.

Araguas-Araguas, L.J., Diaz Teijeiro, M.F., 2005. Isotope composition of precipitation and water vapour in the Iberian Peninsula. First results of the Spanish Network of Isotopes in Precipitation, Isotopic composition of precipitation in the Mediterranean Basin in relation to air circulation patterns and climate. IAEA-TECDOC-1453, Vienna, pp. 173-190.

Baas, M., Pancost, R., van Geel, B., Sinninghe Damsté, J.S., 2000. A comparative study of lipids in Sphagnum species. Organic Geochemistry 31, 535-541.

Báez, J.C., Gimeno, L., Gómez-Gesteira, M., Ferri-Yáñez, F., Real, R., 2013. Combined Effects of the North Atlantic Oscillation and the Arctic Oscillation on Sea Surface Temperature in the Alborán Sea. PLOS ONE 8, e62201.

Barea-Arco, J., Pérez-Martínez, C., Morales-Baquero, R., 2001. Evidence of a mutualistic relationship between an algal epibiont and its host, *Daphnia pulicaria*. Limnology and Oceanography 46, 871-881.

Blaauw, M., Christen, J.A., 2011. Flexible paleoclimate age-depth models using an autoregressive gamma process. Bayesian Anal. 6, 457-474.

Blanca, G., 2001. Flora amenazada y endémica de Sierra Nevada. Consejería de Medio Ambiente de la Junta de Andalucía and University of Granada.

1219 Bowen, G.J., 2020. The Online Isotopes in Precipitation Calculator, version
1220 3.1. http://www.waterisotopes.org.
1221 Brassell, S.C., Eglinton, G., Marlowe, I.T., Pflaumann, U., Sarnthein, M.,
1222 1986. Molecular stratigraphy: a new tool for climatic assessment. Nature
1223 320, 129.
1224 Bray, E.E., Evans, E.D., 1961. Distribution of n-paraffins as a clue to
1225 recognition of source beds. Geochimica et Cosmochimica Acta 22, 2-15.
1226 Bush, R.T., McInerney, F.A., 2013. Leaf wax *n*-alkane distributions in and
1227 across modern plants: Implications for paleoecology and
1228 chemotaxonomy. Geochimica et Cosmochimica Acta 117, 161-179.
1229 Cacho, I., Grimalt, J.O., Pelejero, C., Canals, M., Sierro, F.J., Flores, J.A.,
1230 Shackleton, N., 1999. Dansgaard‐Oeschger and Heinrich event imprints
1231 in Alboran Sea paleotemperatures. Paleoceanography 14, 698-705.
1232 Calvo, E., Pelejero, C., Logan, G.A., De Deckker, P., 2004. Dust-induced
1233 changes in phytoplankton composition in the Tasman Sea during the last
1234 four glacial cycles. Paleoceanography 19, n/a-n/a.
1235 Caseldine, C., Geirsdóttir, Á., Langdon, P., 2003. Efstadalsvatn – a multi-
1236 proxy study of a Holocene lacustrine sequence from NW Iceland.
1237 Journal of Paleolimnology 30, 55-73.
1238 Castañeda, I.S., Schefuß, E., Pätzold, J., Damsté, J.S.S., Weldeab, S.,
1239 Schouten, S., 2010. Millennial‐scale sea surface temperature changes in
1240 the eastern Mediterranean (Nile River Delta region) over the last 27,000
1241 years. Paleoceanography 25.
1242 Celle-Jeanton, H., Travi, Y., Blavoux, B., 2001. Isotopic typology of the
1243 precipitation in the Western Mediterranean Region at three different time
1244 scales. Geophysical Research Letters 28, 1215-1218.
1245 Collins, J.A., Schefuß, E., Mulitza, S., Prange, M., Werner, M., Tharammal, T.,
1246 Paul, A., Wefer, G., 2013. Estimating the hydrogen isotopic composition
1247 of past precipitation using leaf-waxes from western Africa. Quaternary
1248 Science Reviews 65, 88-101.
1249 Combourieu Nebout, N., Peyron, O., Dormoy, I., 2009. Rapid climatic
1250 variability in the west Mediterranean during the last 25 000 years from
1251 high resolution pollen data. Climate of the Past Discussions 5, 671–707.
1252 Craig, H., 1961. Isotopic Variations in Meteoric Waters. Science 133, 1702-
1253 1703.
1254 Cranwell, P.A., Eglinton, G., Robinson, N., 1987. Lipids of aquatic organisms
1255 as potential contributors to lacustrine sediments—II. Organic
1256 Geochemistry 11, 513-527.
1257 D'Errico, M., Yiou, P., Nardini, C., Lunkeit, F., Faranda, D., 2019. Warmer
1258 Mediterranean temperatures do not decrease snowy cold spell intensity
1259 over Italy. HAL Id hal-02367559.
1260 deMenocal, P., Ortiz, J., Guilderson, T., Adkins, J., Sarnthein, M., Baker, L.,
1261 Yarusinsky, M., 2000. Abrupt onset and termination of the African Humid

Period:: rapid climate responses to gradual insolation forcing. Quaternary Science Reviews 19, 347-361.
Diefendorf, A.F., Freeman, K.H., Wing, S.L., Graham, H.V., 2011. Production of n-alkyl lipids in living plants and implications for the geologic past. Geochimica et Cosmochimica Acta 75, 7472-7485.
Diefendorf, A.F., Freimuth, E.J., 2017. Extracting the most from terrestrial plant-derived n-alkyl lipids and their carbon isotopes from the sedimentary record: A review. Organic Geochemistry 103, 1-21.
Dodd, R.S., Poveda, M.M., 2003. Environmental gradients and population divergence contribute to variation in cuticular wax composition in *Juniperus communis*. Biochemical Systematics and Ecology 31, 1257-1270.
Eglinton, G., Hamilton, R.J., 1967. Leaf Epicuticular Waxes. Science 156, 1322-1335.
Eglinton, T.I., Eglinton, G., 2008. Molecular proxies for paleoclimatology. Earth and Planetary Science Letters 275, 1-16.
Eglinton, T.I., Eglinton, G., Dupont, L., Sholkovitz, E.R., Montluçon, D., Reddy, C.M., 2002. Composition, age, and provenance of organic matter in NW African dust over the Atlantic Ocean. Geochemistry, Geophysics, Geosystems 3, 1-27.
Esteban-Parra, M.J., Rodrigo, F.S., Castro-Diez, Y., 1998. Spatial and temporal patterns of precipitation in Spain for the period 1880–1992. International Journal of Climatology 18, 1557-1574.
Ficken, K.J., Li, B., Swain, D.L., Eglinton, G., 2000. An *n*-alkane proxy for the sedimentary input of submerged/floating freshwater aquatic macrophytes. Organic Geochemistry 31, 745-749.
Fletcher, W.J., Debret, M., Goñi, M.F.S., 2013. Mid-Holocene emergence of a low-frequency millennial oscillation in western Mediterranean climate: Implications for past dynamics of the North Atlantic atmospheric westerlies. The Holocene 23, 153-166.
García-Alix, A., 2015. A multiproxy approach for the reconstruction of ancient continental environments. The case of the Mio–Pliocene deposits of the Granada Basin (southern Iberian Peninsula). Global and Planetary Change 131, 1-10.
García-Alix, A., Delgado Huertas, A., Martín Suárez, E., 2012a. Unravelling the Late Pleistocene habitat of the southernmost woolly mammoths in Europe. Quaternary Science Reviews 32, 75-85.
Garcia-Alix, A., Jimenez Espejo, F.J., Toney, J.L., Jiménez-Moreno, G., Ramos-Román, M.J., Anderson, R.S., Ruano, P., Queralt, I., Delgado Huertas, A., Kuroda, J., 2017. Alpine bogs of southern Spain show human-induced environmental change superimposed on long-term natural variations. Scientific Reports 7, 7439
García-Alix, A., Jiménez-Espejo, F.J., Jiménez-Moreno, G., Toney, J.L., Ramos-Román, M.J., Camuera, J., Anderson, R.S., Delgado-Huertas,

A., Martínez-Ruiz, F., Queralt, I., 2018. Holocene geochemical footprint from Semi-arid alpine wetlands in southern Spain. Scientific Data 5, 180024.
Garcia-Alix, A., Jimenez-Espejo, F.J., Lozano, J.A., Jimenez-Moreno, G., Martinez-Ruiz, F., Garcia Sanjuan, L., Aranda Jimenez, G., Garcia Alfonso, E., Ruiz-Puertas, G., Anderson, R.S., 2013. Anthropogenic impact and lead pollution throughout the Holocene in Southern Iberia. Science of the Total Environment 449, 451-460.
García-Alix, A., Jiménez-Moreno, G., Anderson, R.S., Jiménez Espejo, F.J., Delgado Huertas, A., 2012b. Holocene environmental change in southern Spain deduced from the isotopic record of a high-elevation wetland in Sierra Nevada. Journal of Paleolimnology 48, 471-484.
García-Alix, A., Toney, J.L., Jiménez-Moreno, G., Pérez-Martínez, C., Jiménez, L., Rodrigo-Gámiz, M., Anderson, R.S., Camuera, J., Jiménez-Espejo, F.J., Peña-Angulo, D., Ramos-Román, M.J., 2020. Algal lipids reveal unprecedented warming rates in alpine areas of SW Europe during the Industrial Period. Clim. Past 16, 245-263.
Gelpi, E., Schneider, H., Mann, J., Oró, J., 1970. Hydrocarbons of geochemical significance in microscopic algae. Phytochemistry 9, 603-612.
Gimeno, L., Nieto, R., Trigo, R.M., Vicente-Serrano, S.M., López-Moreno, J.I., 2010. Where Does the Iberian Peninsula Moisture Come From? An Answer Based on a Lagrangian Approach. Journal of Hydrometeorology 11, 421-436.
Giorgi, F., 2006. Climate change hot-spots. Geophysical Research Letters 33.
Grassi, B., Redaelli, G., Visconti, G., 2013. Arctic Sea Ice Reduction and Extreme Climate Events over the Mediterranean Region. Journal of Climate 26, 10101-10110.
Heegaard, E., Birks, H.J.B., Telford, R.J., 2005. Relationships between calibrated ages and depth in stratigraphical sequences: an estimation procedure by mixed-effect regression. The Holocene 15, 612-618.
Hemingway, J.D., Schefuß, E., Dinga, B.J., Pryer, H., Galy, V.V., 2016. Multiple plant-wax compounds record differential sources and ecosystem structure in large river catchments. Geochimica et Cosmochimica Acta 184, 20-40.
Hou, J., Huang, Y., Wang, Y., Shuman, B., Oswald, W.W., Faison, E., Foster, D.R., 2006. Postglacial climate reconstruction based on compound-specific D/H ratios of fatty acids from Blood Pond, New England. Geochemistry, Geophysics, Geosystems 7, n/a-n/a.
Huang, Y., Dupont, L., Sarnthein, M., Hayes, J.M., Eglinton, G., 2000. Mapping of C4 plant input from North West Africa into North East Atlantic sediments. Geochimica et Cosmochimica Acta 64, 3505-3513.
Hurrell, J.W., 1995. Decadal Trends in the North Atlantic Oscillation: Regional Temperatures and Precipitation. Science 269, 676-679.

IAEA, 2001. GNIP Maps and Animations. International Atomic Energy Agency, Vienna.

IPCC, 2013. Climate Change 2013: The Physical Science Basis. Contribution of Working Group I to the Fifth Assessment Report of the Intergovernmental Panel on Climate Change. Cambridge University Press, Cambridge, United Kingdom and New York, USA.

IPCC, 2014. Climate Change 2014: Impacts, Adaptation, and Vulnerability. Part B: Regional Aspects. Contribution of Working Group II to the Fifth Assessment Report of the Intergovernmental Panel on Climate Change. Cambridge University Press, Cambridge, United Kingdom and New York, NY, USA.

Jacob, J., Huang, Y., Disnar, J.-R., Sifeddine, A., Boussafir, M., Spadano Albuquerque, A.L., Turcq, B., 2007. Paleohydrological changes during the last deglaciation in Northern Brazil. Quaternary Science Reviews 26, 1004-1015.

Jiménez, L., Conde-Porcuna, J.M., García-Alix, A., Toney, J.L., Anderson, R.S., Heiri, O., Pérez-Martínez, C., 2019. Ecosystem Responses to Climate-Related Changes in a Mediterranean Alpine Environment Over the Last ~ 180 Years. Ecosystems 22, 563-577.

Jiménez, L., Rühland, K.M., Jeziorski, A., Smol, J.P., Pérez-Martínez, C., 2018. Climate change and Saharan dust drive recent cladoceran and primary production changes in remote alpine lakes of Sierra Nevada, Spain. Global Change Biology 28, e139–e158.

Jiménez-Espejo, F.J., García-Alix, A., Jiménez-Moreno, G., Rodrigo-Gámiz, M., Anderson, R.S., Rodríguez-Tovar, F.J., Martínez-Ruiz, F., Giralt, S., Delgado Huertas, A., Pardo-Igúzquiza, E., 2014. Saharan aeolian input and effective humidity variations over western Europe during the Holocene from a high altitude record. Chemical Geology 374-375, 1-12.

Jiménez-Moreno, G., Anderson, R.S., 2012. Holocene vegetation and climate change recorded in alpine bog sediments from the Borreguiles de la Virgen, Sierra Nevada, southern Spain. Quaternary Research 77, 44-53.

Jiménez-Moreno, G., García-Alix, A., Hernández-Corbalán, M.D., Anderson, R.S., Delgado-Huertas, A., 2013. Vegetation, fire, climate and human disturbance history in the southwestern Mediterranean area during the late Holocene. Quaternary Research 79, 110-122.

Kawamura, K., Ishimura, Y., Yamazaki, K., 2003. Four years' observations of terrestrial lipid class compounds in marine aerosols from the western North Pacific. Global Biogeochemical Cycles 17, 3-1-3-19.

Killops, S., Killops, V., 2005. Introduction to Organic Geochemistry. Wiley-Blackwell.

Koenigk, T., Gao, Y., Gastineau, G., Keenlyside, N., Nakamura, T., Ogawa, F., Orsolini, Y., Semenov, V., Suo, L., Tian, T., Wang, T., Wettstein, J.J., Yang, S., 2019. Impact of Arctic sea ice variations on winter temperature anomalies in northern hemispheric land areas. Climate Dynamics 52,

3111-3137.
Krklec, K., Domínguez-Villar, D., 2014. Quantification of the impact of moisture source regions on the oxygen isotope composition of precipitation over Eagle Cave, central Spain. Geochimica et Cosmochimica Acta 134, 39-54.
Kvenvolden, K.A., 1966. Molecular Distributions of Normal Fatty Acids and Paraffins in Some Lower Cretaceous Sediments. Nature 209, 573-577.
Laskar, J., Robutel, P., Joutel, F., Gastineau, M., Correia, A.C.M., Levrard, B., 2004. A long-term numerical solution for the insolation quantities of the Earth. Astronomy and Astrophysics 428, 261-285.
Lattaud, J., Lo, L., Huang, J.-J., Chou, Y.-M., Gorbarenko, S.A., Sinninghe Damsté, J.S., Schouten, S., 2018. A Comparison of Late Quaternary Organic Proxy-Based Paleotemperature Records of the Central Sea of Okhotsk. Paleoceanography and Paleoclimatology 33, 732-744.
Leng, M.J., Marshall, J.D., 2004. Palaeoclimate interpretation of stable isotope data from lake sediment archives. Quaternary Science Reviews 23, 811-831.
Lionello, P., Malanotte-Rizzoli, P., Boscolo, R., Alpert, P., Artale, V., Li, L., Luterbacher, J., May, W., Trigo, R., Tsimplis, M., Ulbrich, U., Xoplaki, E., 2006. The Mediterranean climate: An overview of the main characteristics and issues, Developments in Earth and Environmental Sciences, pp. 1-26.
Liu, J., Curry, J.A., Wang, H., Song, M., Horton, R.M., 2012. Impact of declining Arctic sea ice on winter snowfall. Proceedings of the National Academy of Sciences 109, 4074-4079.
López-Moreno, J.I., Vicente-Serrano, S.M., Morán-Tejeda, E., Lorenzo-Lacruz, J., Kenawy, A., Beniston, M., 2011. Effects of the North Atlantic Oscillation (NAO) on combined temperature and precipitation winter modes in the Mediterranean mountains: Observed relationships and projections for the 21st century. Global and Planetary Change 77, 62-76.
Martin-Vide, J., Lopez-Bustins, J.A., 2006. The Western Mediterranean Oscillation and rainfall in the Iberian Peninsula. International Journal of Climatology 26, 1455-1475.
Martrat, B., Grimalt, J.O., Lopez-Martinez, C., Cacho, I., Sierro, F.J., Flores, J.A., Zahn, R., Canals, M., Curtis, J.H., Hodell, D.A., 2004. Abrupt Temperature Changes in the Western Mediterranean over the past 250,000 Years. Science 306, 1762-1765.
Mesa-Fernández, J.M., Jiménez-Moreno, G., Rodrigo-Gámiz, M., García-Alix, A., Jiménez-Espejo, F.J., Martínez-Ruiz, F., Anderson, R.S., Camuera, J., Ramos-Román, M.J., 2018. Vegetation and geochemical responses to Holocene rapid climate change in the Sierra Nevada (southeastern Iberia): the Laguna Hondera record. Clim. Past 14, 1687-1706.
Millán, M.M., Estrela, M.J., Sanz, M.J., Mantilla, E., Martín, M., Pastor, F.,

Salvador, R., Vallejo, R., Alonso, L., Gangoiti, G., Ilardia, J.L., Navazo, M., Albizuri, A., Artíñano, B., Ciccioli, P., Kallos, G., Carvalho, R.A., Andrés, D., Hoff, A., Werhahn, J., Seufert, G., Versino, B., 2005. Climatic Feedbacks and Desertification: The Mediterranean Model. Journal of Climate 18, 684-701.

Mladenov, N., Sommaruga, R., Morales-Baquero, R., Laurion, I., Camarero, L., Diéguez, M.C., Camacho, A., Delgado, A., Torres, O., Chen, Z., Felip, M., Reche, I., 2011. Dust inputs and bacteria influence dissolved organic matter in clear alpine lakes. Nature Communications 2, 405.

Moossen, H., Abell, R., Quillmann, U., Bendle, J., 2013. Holocene changes in marine productivity and terrestrial organic carbon inputs into an Icelandic fjord: Application of molecular and bulk organic proxies. The Holocene 23, 1699-1710.

Moossen, H., Bendle, J., Seki, O., Quillmann, U., Kawamura, K., 2015. North Atlantic Holocene climate evolution recorded by high-resolution terrestrial and marine biomarker records. Quaternary Science Reviews 129, 111-127.

Morales-Baquero, R., Carrillo, P., Reche, I., Sánchez-Castillo, P., 1999. Nitrogen–phosphorus relationship in high mountain lakes: effects of the size of catchment basins. Can. J. Fish. Aquat. Sci. 56, 1809–1817.

Moreno, A., Pérez, A., Frigola, J., Nieto-Moreno, V., Rodrigo-Gámiz, M., Martrat, B., González-Sampériz, P., Morellón, M., Martín-Puertas, C., Corella, J.P., Belmonte, Á., Sancho, C., Cacho, I., Herrera, G., Canals, M., Grimalt, J.O., Jiménez-Espejo, F., Martínez-Ruiz, F., Vegas-Vilarrúbia, T., Valero-Garcés, B.L., 2012. The Medieval Climate Anomaly in the Iberian Peninsula reconstructed from marine and lake records. Quaternary Science Reviews 43, 16-32.

Moreno, A., Sancho, C., Bartolomé, M., Oliva-Urcia, B., Delgado-Huertas, A., Estrela, M.J., Corell, D., López-Moreno, J.I., Cacho, I., 2014. Climate controls on rainfall isotopes and their effects on cave drip water and speleothem growth: the case of Molinos cave (Teruel, NE Spain). Climate Dynamics 43, 221-241.

Niedermeyer, E.M., Forrest, M., Beckmann, B., Sessions, A.L., Mulch, A., Schefuß, E., 2016. The stable hydrogen isotopic composition of sedimentary plant waxes as quantitative proxy for rainfall in the West African Sahel. Geochimica et Cosmochimica Acta 184, 55-70.

Niedermeyer, E.M., Schefuß, E., Sessions, A.L., Mulitza, S., Mollenhauer, G., Schulz, M., Wefer, G., 2010. Orbital- and millennial-scale changes in the hydrologic cycle and vegetation in the western African Sahel: insights from individual plant wax δD and δ13C. Quaternary Science Reviews 29, 2996-3005.

Nieto-Moreno, V., Martínez-Ruiz, F., Giralt, S., Jiménez-Espejo, F., Gallego-Torres, D., Rodrigo-Gámiz, M., García-Orellana, J., Ortega-Huertas, M., de Lange, G.J., 2011. Tracking climate variability in the western

Mediterranean during the Late Holocene: a multiproxy approach. Climate of the Past 7, 1395-1414.
O'Leary, M.H., 1988. Carbon Isotopes in Photosynthesis: Fractionation techniques may reveal new aspects of carbon dynamics in plants. BioScience 38, 328-336.
Observatorio del cambio global de Sierra Nevada, 2020. Linaria v1.0. iEcolab – Laboratorio de Ecología Terrestre – Universidad de Granada, http://linaria.obsnev.es.
Oliva, M., Gómez Ortiz, A., Palacios, D., Salvador-Franch, F., Salvà-Catarineu, M., 2014. Environmental evolution in Sierra Nevada (South Spain) since the Last Glaciation, based on multi-proxy records. Quaternary International 353, 195-209.
Oliva, M., Moreno, I., 2008. Sierra nevada, nexo entre dos patrones de teleconexión: la NAO y la WEMO, Cambio Climático Regional y sus Impactos. Publicaciones de la Asociación Española de Climatología, pp. 199-208.
Oliva, M., Ruiz-Fernández, J., Barriendos, M., Benito, G., Cuadrat, J.M., Domínguez-Castro, F., García-Ruiz, J.M., Giralt, S., Gómez-Ortiz, A., Hernández, A., López-Costas, O., López-Moreno, J.I., López-Sáez, J.A., Martínez-Cortizas, A., Moreno, A., Prohom, M., Saz, M.A., Serrano, E., Tejedor, E., Trigo, R., Valero-Garcés, B., Vicente-Serrano, S.M., 2018. The Little Ice Age in Iberian mountains. Earth-Science Reviews 177, 175-208.
Olsen, J., Anderson, N.J., Knudsen, M.F., 2012. Variability of the North Atlantic Oscillation over the past 5,200 years. Nature Geosciences 5, 808-812.
Palade, B., Palacios Estremera, D., Gómez Ortiz, A., 2011. Los glaciares rocosos de Sierra Nevada y su significado paleoclimático : Una primera aproximación. Cuadernos de Investigación Geográfica 37, 95-118.
Pérez-Palazón, M.J., Pimentel, R., Polo, M.J., 2018. Climate Trends Impact on the Snowfall Regime in Mediterranean Mountain Areas: Future Scenario Assessment in Sierra Nevada (Spain). . Water 10, 720.
Pulido-Villena, E., Reche, I., Morales-Baquero, R., 2005. Food web reliance on allochthonous carbon in two high mountain lakes with contrasting catchments: a stable isotope approach. Canadian Journal of Fisheries and Aquatic Sciences 62, 2640–2648
Rach, O., Kahmen, A., Brauer, A., Sachse, D., 2017. A dual-biomarker approach for quantification of changes in relative humidity from sedimentary lipid D/H ratios. Clim. Past 13, 741-757.
Ramos-Román, M.J., Jiménez-Moreno, G., Camuera, J., García-Alix, A., Scott Anderson, R., Jiménez-Espejo, F.J., Sachse, D., Toney, J.L., Carrión, J.S., Webster, C., Yanes, Y., 2018. Millennial-scale cyclical environment and climate variability during the Holocene in the western Mediterranean region deduced from a new multi-proxy analysis from the

Padul record (Sierra Nevada, Spain). Global and Planetary Change 168, 35-53.
Ramos-Román, M.J., Jiménez-Moreno, G., R.S., A., García-Alix, A., Toney, J.L., Jiménez-Espejo, F.J., Carrión, J.S., 2016. Centennial-scale vegetation and North Atlantic Oscillation changes during the Late Holocene in the southern Iberia. Quaternary Science Reviews 143, 84-95.
Rampen, S.W., Datema, M., Rodrigo-Gámiz, M., Schouten, S., Reichart, G.-J., Sinninghe Damsté, J.S., 2014. Sources and proxy potential of long chain alkyl diols in lacustrine environments. Geochimica et Cosmochimica Acta 144, 59-71.
Rampen, S.W., Schouten, S., Sinninghe Damsté, J.S., 2011. Occurrence of long chain 1,14-diols in *Apedinella radians*. Organic Geochemistry 42, 572-574.
Rampen, S.W., Willmott, V., Kim, J.-H., Uliana, E., Mollenhauer, G., Schefuß, E., Sinninghe Damsté, J.S., Schouten, S., 2012. Long chain 1,13- and 1,15-diols as a potential proxy for palaeotemperature reconstruction. Geochimica et Cosmochimica Acta 84, 204-216.
Raya Garrido, J., 2003. Composición isotópica del vapor de agua atmosférico en el sureste de la Península Ibérica. Editorial de la Universidad de Granada, Granada.
Reche, I., Ortega-Retuerta, E., Romera, O., Pulido-Villena, E., Morales-Baquero, R., Casamayor, E.O., 2009. Effect of Saharan dust inputs on bacterial activity and community composition in Mediterranean lakes and reservoirs. Limnol. Oceanogr 54, 869–879.
Reimer, P.J., Bard, E., Bayliss, A., Beck, J.W., Blackwell, P.G., Ramsey, C.B., Buck, C.E., Cheng, H., Edwards, R.L., Friedrich, M., Grootes, P.M., Guilderson, T.P., Haflidason, H., Hajdas, I., Hatté, C., Heaton, T.J., Hoffmann, D.L., Hogg, A.G., Hughen, K.A., Kaiser, K.F., Kromer, B., Manning, S.W., Niu, M., Reimer, R.W., Richards, D.A., Scott, E.M., Southon, J.R., Staff, R.A., Turney, C.S.M., van der Plicht, J., 2013. IntCal13 and Marine13 Radiocarbon Age Calibration Curves 0–50,000 Years cal. BP. Radiocarbon 55, 1869-1887.
Rodrigo, F.S., Esteban-Parra, M.J., Pozo-Vázquez, D., Castro-Díez, Y., 1999. A 500-year precipitation record in Southern Spain. International Journal of Climatology 19, 1233-1253.
Rodrigo-Gámiz, M., Martínez-Ruiz, F., Rampen, S.W., Schouten, S., Damsté, J.S.S., 2014. Sea surface temperature variations in the western Mediterranean Sea over the last 20 kyr: A dual-organic proxy (UK′37 and LDI) approach. Paleoceanography 29, 87-98.
Ryan, W.B.F., Carbotte, S.M., Coplan, J.O., O'Hara, S., Melkonian, A., Arko, R., Weissel, R.A., Ferrini, V., Goodwillie, A., Nitsche, F., Bonczkowski,

J., Zemsky, R., 2009. Global Multi-Resolution Topography synthesis. Geochemistry, Geophysics, Geosystems 10.

Sachse, D., Billault, I., Bowen, G.J., Chikaraishi, Y., Dawson, T.E., Feakins, S.J., Freeman, K.H., Magill, C.R., McInerney, F.A., Meer, M.T.J.v.d., Polissar, P., Robins, R.J., Sachs, J.P., Schmidt, H.-L., Sessions, A.L., White, J.W.C., West, J.B., Kahmen, A., 2012. Molecular Paleohydrology: Interpreting the Hydrogen-Isotopic Composition of Lipid Biomarkers from Photosynthesizing Organisms. Annual Review of Earth and Planetary Sciences 40, 221-249.

Sachse, D., Radke, J., Gleixner, G., 2004. Hydrogen isotope ratios of recent lacustrine sedimentary *n*-alkanes record modern climate variability. Geochimica et Cosmochimica Acta 68, 4877-4889.

Sachse, D., Radke, J., Gleixner, G., 2006. δD values of individual *n*-alkanes from terrestrial plants along a climatic gradient – Implications for the sedimentary biomarker record. Organic Geochemistry 37, 469-483.

Sánchez-Castillo, P.M., 1988. Algas de las lagunas de alta montaña de Sierra Nevada (Granada, España). Acta Botánica Malacitana 13, 21 -52.

Schefuß, E., Ratmeyer, V., Stuut, J.-B.W., Jansen, J.H.F., Sinninghe Damsté, J.S., 2003a. Carbon isotope analyses of *n*-alkanes in dust from the lower atmosphere over the central eastern Atlantic. Geochimica et Cosmochimica Acta 67, 1757-1767.

Schefuß, E., Schouten, S., Jansen, J.H.F., Sinninghe Damsté, J.S., 2003b. African vegetation controlled by tropical sea surface temperatures in the mid-Pleistocene period. Nature 422, 418.

Seki, O., Meyers, P.A., Yamamoto, S., Kawamura, K., Nakatsuka, T., Zhou, W., Zheng, Y., 2011. Plant-wax hydrogen isotopic evidence for postglacial variations in delivery of precipitation in the monsoon domain of China. Geology 39, 875-878.

Seki, O., Nakatsuka, T., Shibata, H., Kawamura, K., 2010. A compound-specific *n*-alkane δ13C and δD approach for assessing source and delivery processes of terrestrial organic matter within a forested watershed in northern Japan. Geochimica et Cosmochimica Acta 74, 599-613.

Shimokawara, M., Nishimura, M., Matsuda, T., Akiyama, N., Kawai, T., 2010. Bound forms, compositional features, major sources and diagenesis of long chain, alkyl mid-chain diols in Lake Baikal sediments over the past 28,000 years. Organic Geochemistry 41, 753-766.

Sinninghe Damsté, J.S., Rampen, S., Irene, W., Rijpstra, C., Abbas, B., Muyzer, G., Schouten, S., 2003. A diatomaceous origin for long-chain diols and mid-chain hydroxy methyl alkanoates widely occurring in quaternary marine sediments: indicators for high-nutrient conditions. Geochimica et Cosmochimica Acta 67, 1339-1348.

Smith, M., De Deckker, P., Rogers, J., Brocks, J., Hope, J., Schmidt, S.,

Lopes dos Santos, R., Schouten, S., 2013. Comparison of U37K′, TEX86H and LDI temperature proxies for reconstruction of south-east Australian ocean temperatures. Organic Geochemistry 64, 94-104.
Spanish National Weather Agency - AEMet Open Data, 2020. AEMet Open Data, http://www.aemet.es/es/datos_abiertos/AEMET_OpenData.
Tierney, J.E., Pausata, F.S.R., deMenocal, P.B., 2017. Rainfall regimes of the Green Sahara. Science Advances 3, e1601503.
Tipple, B.J., Pagani, M., 2007. The Early Origins of Terrestrial C4 Photosynthesis. Annual Review of Earth and Planetary Sciences 35, 435-461.
Toney, J.L., Huang, Y., Fritz, S.C., Baker, P.A., Grimm, E., Nyren, P., 2010. Climatic and environmental controls on the occurrence and distributions of long chain alkenones in lakes of the interior United States. Geochimica et Cosmochimica Acta 74, 1563-1578.
Trigo, R., Xoplaki, E., Zorita, E., Luterbacher, J., Krichak, S.O., Alpert, P., Jacobeit, J., Sáenz, J., Fernández, J., González-Rouco, F., Garcia-Herrera, R., Rodo, X., Brunetti, M., Nanni, T., Maugeri, M., Türke§, M., Gimeno, L., Ribera, P., Brunet, M., Trigo, I.F., Crepon, M., Mariotti, A., 2006. Chapter 3 Relations between variability in the Mediterranean region and mid-latitude variability, in: Lionello, P., Malanotte-Rizzoli, P., Boscolo, R. (Eds.), Developments in Earth and Environmental Sciences. Elsevier, pp. 179-226.
Trouet, V., Esper, J., Graham, N.E., Baker, A., Scourse, J.D., Frank, D.C., 2009. Persistent Positive North Atlantic Oscillation Mode Dominated the Medieval Climate Anomaly. Science 324, 78-80.
Valle, F., 2003. Mapa de Series de Vegetación de Andalucía. Editorial Rueda, S.I., Madrid.
Van Swaay, C.A.M., Warren, M.S., 1999. Red Data book of European butterflies (Rhopalocera). Council of Europe Publishing, Strasbourg.
Vihma, T., 2014. Effects of Arctic Sea Ice Decline on Weather and Climate: A Review. Surveys in Geophysics 35, 1175-1214.
Villanueva, L., Besseling, M., Rodrigo-Gámiz, M., Rampen, S.W., Verschuren, D., Sinninghe Damsté, J.S., 2014. Potential biological sources of long chain alkyl diols in a lacustrine system. Organic Geochemistry 68, 27-30.
Vogts, A., Moossen, H., Rommerskirchen, F., Rullkötter, J., 2009. Distribution patterns and stable carbon isotopic composition of alkanes and alkan-1-ols from plant waxes of African rain forest and savanna C3 species. Organic Geochemistry 40, 1037-1054.
Vonk, J.E., Gustafsson, Ö., 2009. Calibrating *n*-alkane *Sphagnum* proxies in sub-Arctic Scandinavia. Organic Geochemistry 40, 1085-1090.
Walker, M.J.C., Berkelhammer, M., Björck, S., Cwynar, L.C., Fisher, D.A., Long, A.J., Lowe, J.J., Newnham, R.M., Rasmussen, S.O., Weiss, H., 2012. Formal subdivision of the Holocene Series/Epoch: a Discussion Paper by a Working Group of INTIMATE (Integration of ice-core, marine

and terrestrial records) and the Subcommission on Quaternary Stratigraphy (International Commission on Stratigraphy). Journal of Quaternary Science 27, 649-659.

Zamora, R., Perez-Luque, A., Bonet, F., Barea-Azcoìn, J., Aspizua, R., 2016. Change impacts in Sierra Nevada: challenges for conservation. Consejeria de Medio Ambiente y Ordenacioìn del Territorio, Junta de Andalucia, Andalucia.

Zhou, W., Xie, S., Meyers, P.A., Zheng, Y., 2005. Reconstruction of late glacial and Holocene climate evolution in southern China from geolipids and pollen in the Dingnan peat sequence. Organic Geochemistry 36, 1272-1284.

FIGURE CAPTIONS

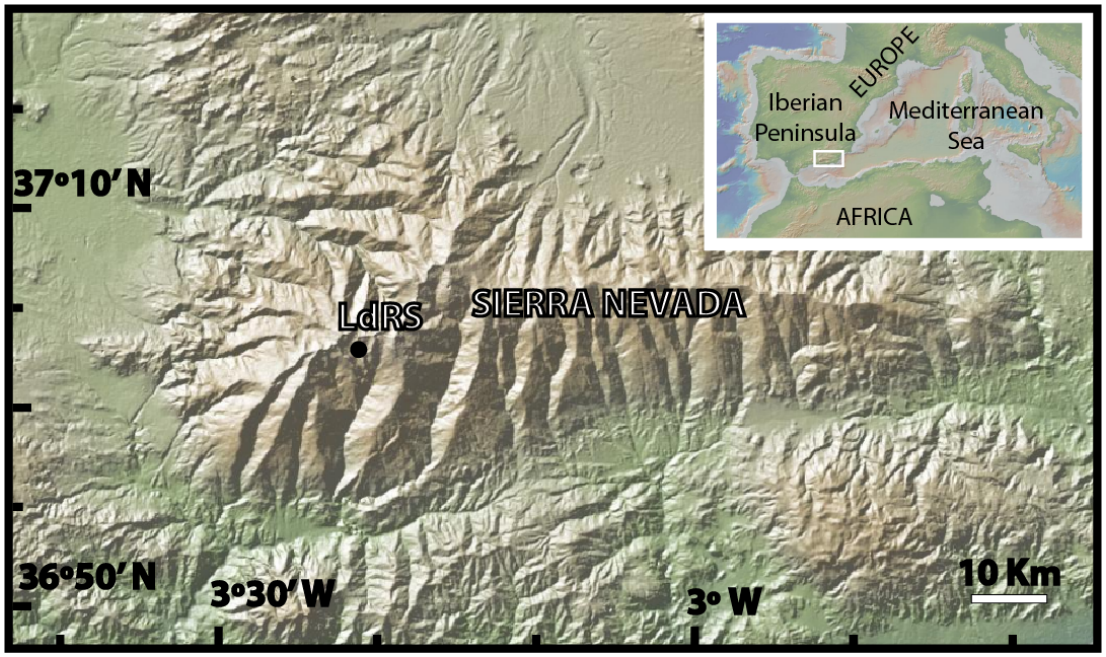

Figure 1. Geographical location of the Sierra Nevada in the western Mediterranean region and Laguna de Río Seco site (LdRS). Map created by A. García-Alix using GeoMapApp (3.6.6) (http://www.geomapapp.org) with the underlying Global Multi-Resolution Topography synthesis map (Ryan et al., 2009).

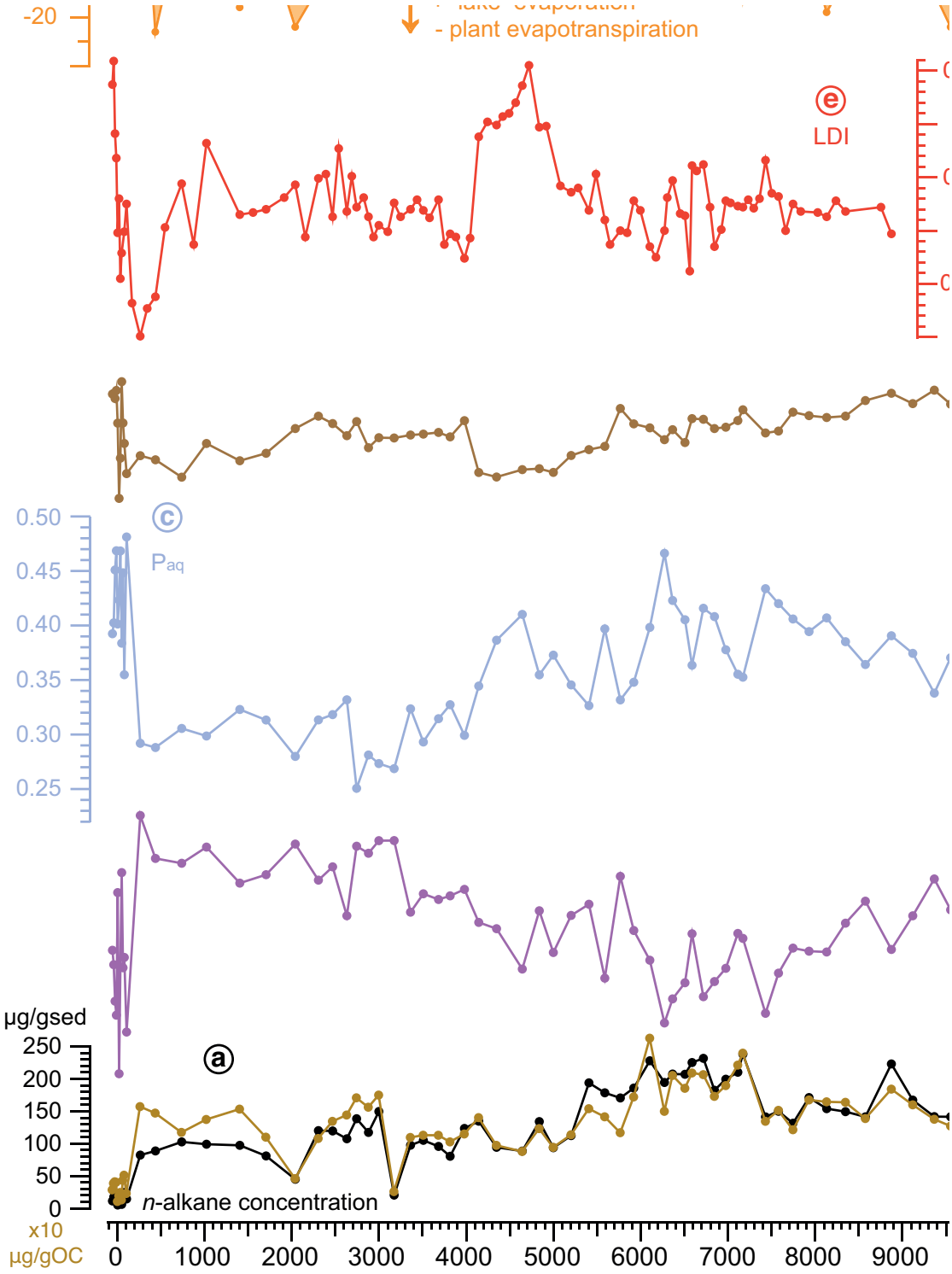

Figure 2. Biomarker proxies studied in LdRS record from 12,300 cal. yr BP to the present. (a) total *n*-alkane concentration in microgram per gram of dry sediment and microgram per gram of organic carbon (µg $gsed^{-1}$ and µg gOC^{-1}); **(b)** average chain length between C_{25} and C_{33} *n*-alkanes (ACL), **(c)** portion aquatic deduced from C_{23}-C_{25}-C_{29} and C_{31} *n*-alkanes (P_{aq}); **(d)** carbon preference index from C_{24} to C_{34} *n*-alkanes (CPI); **(e)** Long-Chain Diol Index (LDI) from C_{28} 1,13-, C_{30}1,13-, and C_{30} 1,15-diols as well as the calibrated

Mean Annual Air Temperatures (MAAT) and Mean Annual Air Temperature Anomalies respect to the reference period 2008-1979 (MAATA); **(f)** ΔD_{wax-aq} calculated from the difference between δD_{wax}-δD_{aq} values; **(g)** hydrogen isotopic composition of the terrestrial C_{29} and C_{31} *n*-alkanes (δD_{wax}); **(h)** hydrogen isotopic composition of the aquatic C_{23} and C_{25} *n*-alkanes (δD_{aq}).

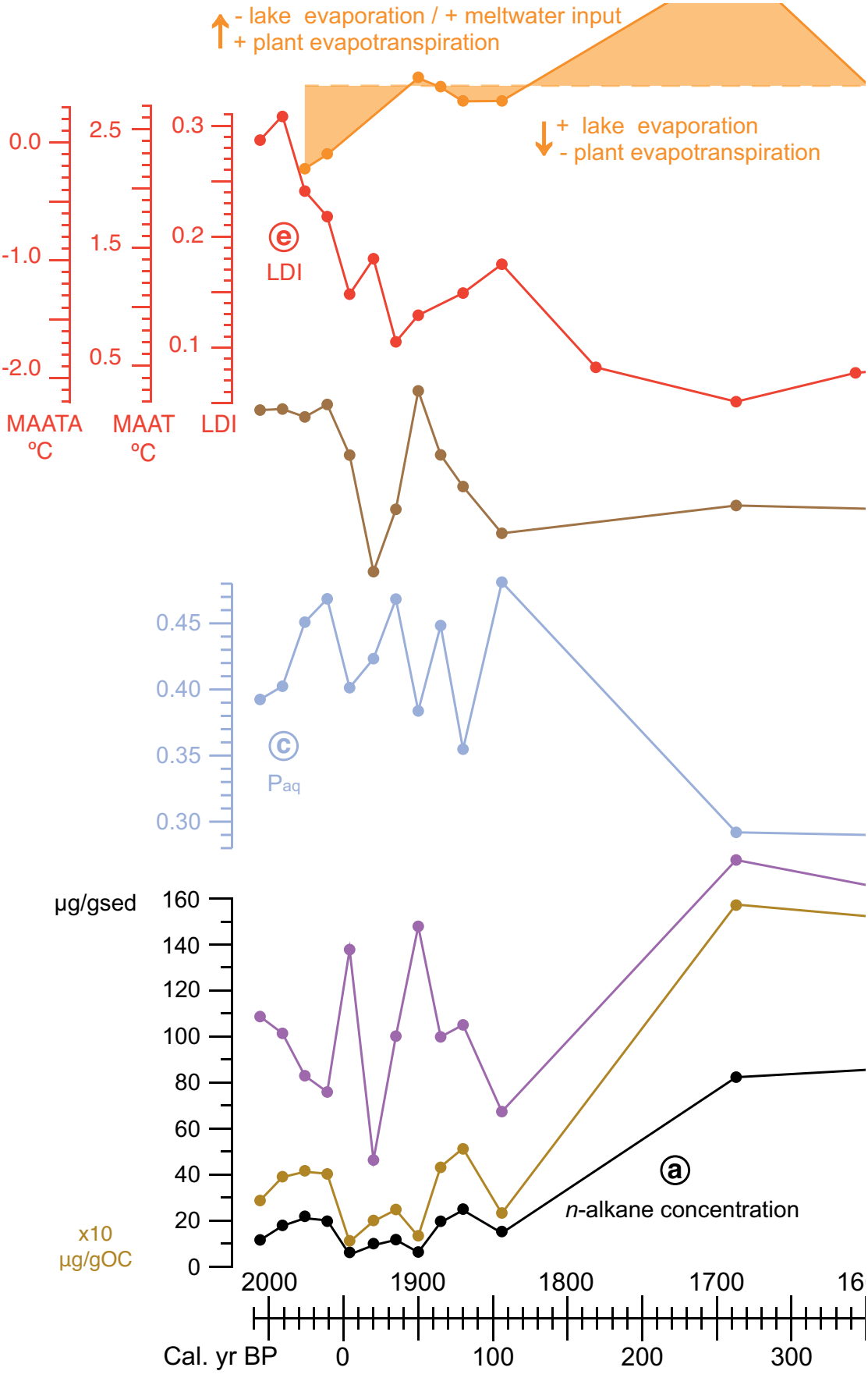
- lake evaporation / + meltwater input
+ plant evapotranspiration
+ lake evaporation
- plant evapotranspiration
0.0
-1.0
-2.0
MAATA °C
2.5
1.5
0.5
MAAT °C
0.3
0.2
0.1
LDI
e
LDI
0.45
0.40
0.35
0.30
c
Paq
µg/gsed
160
140
120
100
80
60
40
20
0
x10 µg/gOC
a
n-alkane concentration
2000
1900
1800
1700
16
Cal. yr BP
0
100
200
300

1688
1689

Figure 3. Detail of the biomarker proxies studied in LdRS record from 500 cal. yr BP to the present along with the reconstructed precipitation anomaly in southern Iberian Peninsula. (a) total *n*-alkane concentration in microgram per gram of dry sediment and microgram per gram of organic carbon (μg $gsed^{-1}$ and μg gOC^{-1}); **(b)** average chain length between C_{25} and C_{33} *n*-alkanes (ACL), **(c)** portion aquatic deduced from C_{23}-C_{25}-C_{29} and C_{31} *n*-alkanes (P_{aq}); **(d)** carbon preference index from C_{24} to C_{34} *n*-alkanes (CPI); **(e)** Long-Chain Diol Index (LDI) from C_{28} 1,13-, C_{30} 1,13-, and C_{30} 1,15-diols as well as the calibrated Mean Annual Air Temperatures (MAAT) and Mean Annual Air Temperature Anomalies respect to the reference period 2008-1979 (MAATA); **(f)** ΔD_{wax-aq} calculated from the difference between δD_{wax} and δD_{aq} values; **(g)** hydrogen isotopic composition of the terrestrial C_{29} and C_{31} *n*-alkanes (δD_{wax}); **(h)** hydrogen isotopic composition of the aquatic C_{23} and C_{25} *n*-alkanes (δD_{aq}); **(i)** reconstruction of the precipitation anomaly in southern Iberian Peninsula for the last 500 years (Rodrigo et al., 1999).

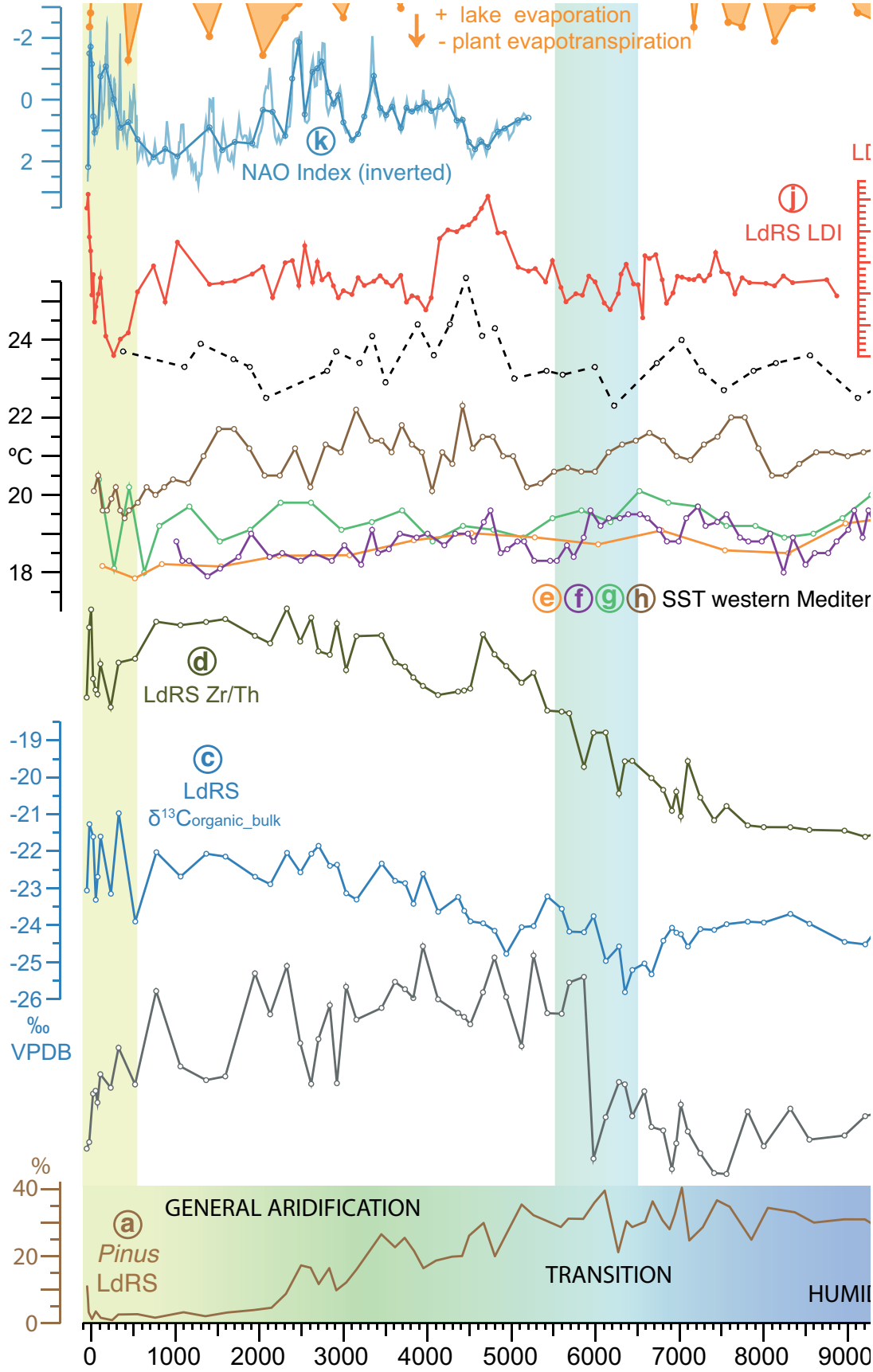

Figure 4. Comparison among the studied results and Northern Hemisphere environmental indices for the last 12,300 years. (a) *Pinus* L.

pollen record in LdRS (Anderson et al., 2011) along with the general regional environmental trend in southern Iberia; **(b)** atomic carbon – nitrogen ratio (C/N) record in LdRS (Jiménez-Espejo et al., 2014); **(c)** bulk organic $\delta^{13}C$ record in LdRS (Jiménez-Espejo et al., 2014); **(d)** zirconium – thorium ratio (Zr/Th) record in LdRS (Jiménez-Espejo et al., 2014); **(e-h)** alkenone sea-surface temperatures from the western Mediterranean: **(e)** core ODP977A (Martrat et al., 2004), **(f)** core MD95-2043 (Cacho et al., 1999), **(g)** core TTR-12_293G (Rodrigo-Gámiz et al., 2014), **(h)** core TTR-17_434G (Rodrigo-Gámiz et al., 2014); **(i)** alkenone sea-surface temperatures from the eastern Mediterranean: core GEOB 770-2 (Castañeda et al., 2010); **(j)** Long-Chain Diol Index (LDI) from C_{28} 1,13-, C_{30} 1,13-, and C_{30} 1,15-diols as well as the calibrated Mean Annual Temperatures (MAT) and Mean Annual Temperature Anomalies respect to the reference period 2008-1979; **(k)** NAO index reconstruction for the last ~5000 years (Olsen et al., 2012; Trouet et al., 2009); (**l)** ΔD_{wax-aq} calculated from the difference between δD_{wax} and δD_{aq} values; **(m)** hydrogen isotopic composition of the terrestrial C_{29} and C_{31} *n*-alkanes (δD_{wax}); **(n)** hydrogen isotopic composition of the aquatic C_{23} and C_{25} *n*-alkanes (δD_{aq}).

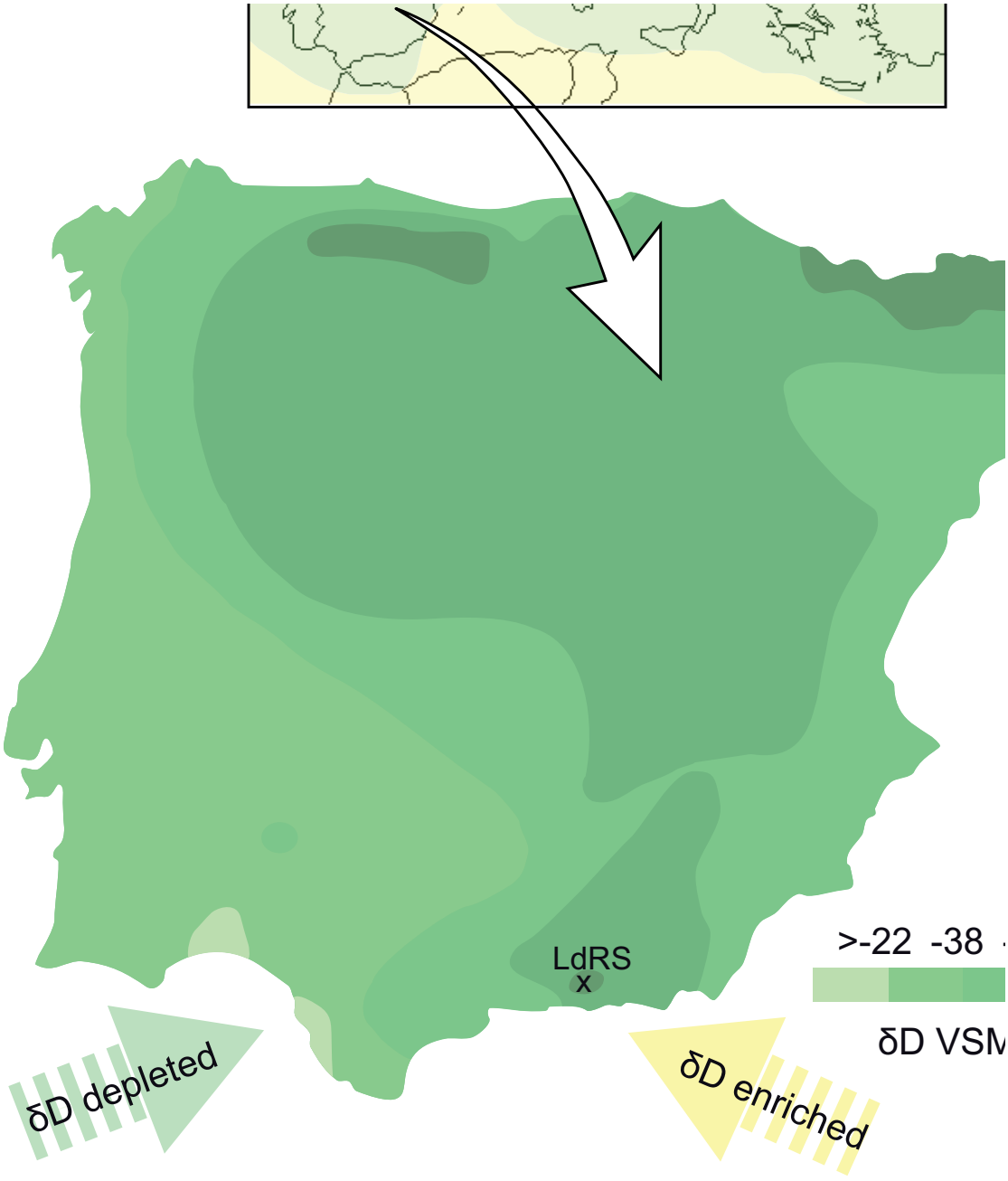

Figure 5. Hydrogen isotopic composition of meteoric waters in Europe. **(a)** general hydrogen isotopic composition of precipitation in Europe (IAEA, 2001); **(b)** distribution map of hydrogen isotopes in precipitation, springs, and shallow water in the Iberian Peninsula (Araguas-Araguas and Diaz Teijeiro, 2005). The hydrogen isotopic composition have been calculated from $\delta^{18}O$ values using the Global Meteoric Water Line: $\delta D = 8.0 \times \delta^{18}O + 10‰$ (Craig, 1961). Note the depleted values coming from Atlantic vapour masses and the isotopically-enriched ones from the Mediterranean ones.

TABLE

Table 1. Pearson correlation matrix between the hydrogen isotopic composition of the different *n*-alkanes analysed in this study. Lower matrix: *r* index; upper matrix: *p* value.

	δDC_{23}	**δDC_{25}**	**δDC_{27}**	**δDC_{29}**	**δDC_{31}**	**δDC_{33}**
δDC_{23}		2.7E-15	2.3E-11	7.2E-09	1.8E-07	8.8E-11
δDC_{25}	0.85		2.3E-21	8.8E-16	2.3E-14	1.1E-13
δDC_{27}	0.77	0.87		7.6E-30	9.9E-21	1.1E-18
δDC_{29}	0.70	0.80	0.93		4.9E-31	1.4E-20
δDC_{31}	0.64	0.78	0.86	0.93		3.3E-16
δDC_{33}	0.79	0.81	0.87	0.89	0.84	